HHS Public Access

Author manuscript

Cell Rep. Author manuscript; available in PMC 2021 November 19.

Published in final edited form as:

Cell Rep. 2020 October 06; 33(1): 108236. doi:10.1016/j.celrep.2020.108236.

Cystatin C Plays a Sex-Dependent Detrimental Role in Experimental Autoimmune Encephalomyelitis

Vahid Hoghooghi[1], **Alexandra L. Palmer**[1], **Ariana Frederick**[2], **Yulan Jiang**[2], **Jessica E. Merkens**[1], **Anjali Balakrishnan**[3], **Trisha M. Finlay**[1], **Anders Grubb**[4], **Efrat Levy**[5,6], **Paul Gordon**[7], **Frank R. Jirik**[8], **Minh Dang Nguyen**[2,9], **Carol Schuurmans**[3], **Frank Visser**[10], **Shannon E. Dunn**[11], **Shalina S. Ousman**[2,12,13,*]

[1]Department of Neuroscience, Hotchkiss Brain Institute, University of Calgary, Calgary, AB T2N 4N1, Canada

[2]Department of Clinical Neurosciences, Hotchkiss Brain Institute, University of Calgary, Calgary, AB T2N 4N1, Canada

[3]Biological Sciences Platform, Sunnybrook Research Institute, Toronto, ON M4N 3M5, Canada

[4]Department of Clinical Chemistry, Lund University Hospital, SE 221 85 Lund, Sweden

[5]Department of Psychiatry and Department of Biochemistry & Molecular Pharmacology, Neuroscience Institute, NYU Langone Health, New York, NY, USA

[6]Nathan S. Kline Institute for Psychiatric Research, Orangeburg, NY 10962, USA

[7]Cumming School of Medicine Centre for Health Genomics and Informatics, University of Calgary, Calgary, AB T2N 4N1, Canada

[8]Department of Biochemistry & Molecular Biology, and Department of Medicine, Alberta Children's Hospital Research Institute, University of Calgary, Calgary, AB T2N 4N1, Canada

[9]Department of Cell Biology & Anatomy, and Department of Biochemistry & Molecular Biology, Hotchkiss Brain Institute, University of Calgary, Calgary, AB T2N 4N1, Canada

[10]Department of Physiology and Pharmacology, Hotchkiss Brain Institute, University of Calgary, Calgary, AB T2N 4N1, Canada

[11]Department of Immunology, Keenan Research Centre for Biomedical Science of St. Michael's Hospital, St. Michael's Hospital, University of Toronto, Toronto, ON M5B 1W8, Canada

*Correspondence: sousman@ucalgary.ca.

AUTHOR CONTRIBUTIONS

S.S.O. conceived the study and experiments and wrote the manuscript. V.H. formulated and performed experiments and analyses. A.L.P., A.F., J.E.M., and T.M.F. assisted with the gonadectomy experiments. F.R.J. participated in experimental design. E.L. and A.G. provided the genetically modified mice and participated in data discussions. C.S. and A.B. performed the *in situ* hybridization, and M.D.N. and Y.J. assisted with western blots. P.G. assisted with RNA-seq analysis, while F.V. created the *Cst3* constructs and performed the transfections. S.E.D. participated in experimental design, data discussion and acquisition, manuscript editing, and provision of some of the intracellular flow cytometry antibodies.

SUPPLEMENTAL INFORMATION

Supplemental Information can be found online at https://doi.org/10.1016/j.celrep.2020.108236.

DECLARATION OF INTERESTS

The authors declare no competing interests.

[12]Department of Cell Biology & Anatomy, Hotchkiss Brain Institute, University of Calgary, Calgary, AB T2N 4N1, Canada

[13]Lead Contact

SUMMARY

The cysteine protease inhibitor Cystatin C (CST3) is highly expressed in the brains of multiple sclerosis (MS) patients and C57BL/6J mice with experimental autoimmune encephalomyelitis (EAE; a model of MS), but its roles in the diseases are unknown. Here, we show that CST3 plays a detrimental function in myelin oligodendrocyte glycoprotein 35–55 ($MOG_{35–55}$)-induced EAE but only in female animals. Female *Cst3* null mice display significantly lower clinical signs of disease compared to wild-type (WT) littermates. This difference is associated with reduced interleukin-6 production and lower expression of key proteins (CD80, CD86, major histocompatibility complex [MHC] II, LC3A/B) involved in antigen processing, presentation, and co-stimulation in antigen-presenting cells (APCs). In contrast, male WT and $Cst3^{-/-}$ mice and cells show no differences in EAE signs or APC function. Further, the sex-dependent effect of CST3 in EAE is sensitive to gonadal hormones. Altogether, we have shown that CST3 has a sex-dependent role in $MOG_{35–55}$-induced EAE.

Graphical Abstract

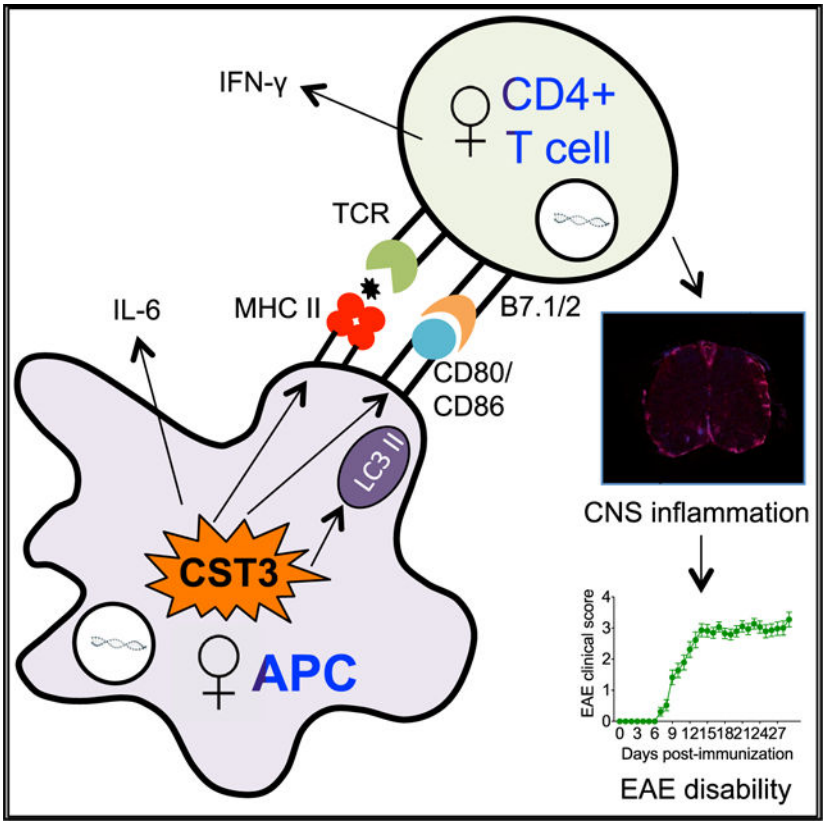

In Brief

Cystatin C (CST3) is increased in the brains of multiple sclerosis patients, but its role is unknown. In a mouse model of the disease, Hoghooghi et al. find that CST3 has a detrimental function but only in female animals. The effect is related to activation of antigen-presenting cells of the immune system.

INTRODUCTION

Multiple sclerosis (MS) is an autoimmune disease of unknown etiology that is characterized by inflammation, demyelination, and axonal degeneration of the central nervous system (CNS). Numerous genes and proteins are upregulated or decreased in the brains of MS patients (Chabas et al., 2001; Han et al., 2008; Lock et al., 2002), but the functions of most of these molecules are poorly understood. These factors may contribute to disease initiation and development, progression, or attempts at resolution. Therefore, understanding the roles of these differentially expressed proteins may lead to the discovery of treatments for the disorder.

Although controversial, Cystatin C (*Cst3*) is a gene that is reported to have enhanced expression in the brains of MS subjects (Chabas et al., 2001; Nakashima et al., 2007). High levels of a cleaved form of the protein were found in the cerebrospinal fluid (CSF) of clinically isolated syndrome (CIS) and CIS-converted to MS patients, and as a consequence, it was proposed that CST3 could serve as a biomarker for the disease (Irani et al., 2006). However, others have reported a decrease in the level of CST3 in MS CSF (Nakashima et al., 2007), and it appears that the presence of CST3 in CSF is not specific to MS, since it can also be upregulated in the CNS in other neuroinflammatory conditions (Del Boccio et al., 2007; Fiorini et al., 2007; Hansson et al., 2007; Nakashima et al., 2007). Similar to findings in the CNS, CST3 has also been reported to be upregulated in peripheral blood lymphocytes of relapsing-remitting MS patients (Haves-Zburof et al., 2011). Despite these multiple reports on its expression, it is currently unknown what role, if any, CST3 plays in MS.

In the CNS and immune system, the functions of CST3 are ambiguous, with both neuroprotective and neurodegenerative as well as immunostimulatory and immunosuppressive properties reported (Bäcklund et al., 2011; El-Sukkari et al., 2003; Frendéus et al., 2009; Gauthier et al., 2011, 2012; Kitamura et al., 2005; Leung-Tack et al., 1990; Mellman and Steinman, 2001; Nagai et al., 2005, 2008; Olsson et al., 2004; Palm et al., 1995; Tizon et al., 2010a, 2010b; Verdot et al., 1996; Warfel et al., 1987; Xu et al., 2005). For instance, CST3 is generally thought to be an endogenous neuroprotective molecule that acts by inhibiting cathepsins that are involved in tissue damage, tumor invasion, and neuronal apoptosis (Gauthier et al., 2011). Larger brain infarcts are seen in *Cst3* knockout (KO) mice after focal ischemia (Olsson et al., 2004), and the decreased levels of CST3 associated with Alzheimer's disease (AD) is speculated to contribute to the oligomerization of amyloid-beta (Aβ) and the formation of amyloid fibrils (Gauthier et al., 2012). Not all studies, however, have demonstrated a neuroprotective effect for CST3. Some studies suggest that CST3 may be a positive regulator of AD pathogenesis because of the colocalization of CST3 with Aβ in the vascular walls of AD brains and within parenchymal

Aβ senile plaques (Itoh et al., 1993; Levy et al., 2001; Maruyama et al., 1990; Vinters et al., 1990). Also, injection of CST3 into the hippocampus and dentate gyrus or *in vitro* application of CST3 revealed a role in mediation of neuronal death (Nagai et al., 2008). Indeed, increased expression of CST3 in glial cells was accompanied by neuronal death (Nagai et al., 2005, 2008), and Olsson et al. (2004) reported reduced brain damage in the CA3 region of the hippocampus, dentate gyrus, and cortex of *Cst3*KO mice after global ischemia.

In regard to the immune system, CST3 is expressed in T cells, B cells, macrophages, and dendritic cells (DCs), and like the CNS, a similar ambiguity in the function of CST3 has been described in this system. For instance, some studies have attributed an anti-activation role for the protease inhibitor. For example, Bäcklund et al. (2011) demonstrated a protective role for CST3 in collagen-induced arthritis (CIA) in that $Cst3^{-/-}$ mice had a higher incidence of the disease that was associated with enhanced T and B cell responses in the priming phase, augmented T cell activation by CIA-derived $Cst3^{-/-}$ antigen-presenting cells (APCs), and hyperactivity of naive $Cst3^{-/-}$ DCs. Also consistent with an immune limiting role, other reports have shown that activation of mouse macrophages with lipopolysaccharide (LPS) or interferon-gamma (IFN-γ) was accompanied by a decrease in CST3 secretion (Frendéus et al., 2009; Warfel et al., 1987). Altogether, these studies indicated that CST3 is associated with immune inactivation. However, Kitamura et al., 2005 showed that decreased CST3 expression was linked to reduced major histocompatibility complex class II (MHC II) expression and inflammation in interleukin-6 (IL-6)-activated DCs, although this pro-inflammatory aspect may be specific to certain functions in DCs, because it has been reported that CST3 does not alter antigen presentation by DCs (El-Sukkari et al., 2003). Further, CST3 plays important roles in the maturation of monocytes and DCs, as well as regulating the function of cathepsins and invariant chain processing in macrophages and DCs (El-Sukkari et al., 2003; Pierre and Mellman, 1998; Rodriguez-Franco et al., 2012; Warfel et al., 1987) that can impact antigen presentation. It is, therefore, possible that the type of and localization of the injury or disease, the environment of the disease or injury, and/or the cell type(s) involved may determine what role CST3 plays in the immune system and nervous system.

Due to the reported upregulation of *CST3* in MS tissues and the contrasting functions of CST3 in the immune system and CNS, we sought to elucidate what role, if any, this protein plays during CNS autoimmunity. Our studies revealed a disease-promoting function for CST3 in female mice in the C57BL/6J myelin oligodendrocyte glycoprotein 35–55 ($MOG_{35–55}$)-induced experimental autoimmune encephalomyelitis (EAE) model of MS. Interestingly, our studies revealed a sex-dependent function of this protein, in that CST3 deficiency had no impact on EAE severity in male mice. These pro-inflammatory activities of CST3 in females were linked to this protein promoting APC function through regulation of IL-6 production and LC3/CD80/CD86/MHC II expression. Further, although CST3 was not differently expressed in males and females, there appears to be a modulatory role for female hormones in its function, since the sex-dependent activities of CST3 were negated by ovariectomy in females or revealed by estrogen/progesterone treatment in males.

RESULTS

CST3 Is Upregulated in the CNS during EAE and MS

Enhanced levels of *CST3* mRNA were previously observed in the brains of MS patients relative to control subjects (Chabas et al., 2001). Here, we confirmed that protein expression of CST3 is also elevated in brain tissue from MS patients (Figure S1A; Table S1). To determine whether CST3 expression is similarly upregulated in the CNS during EAE, we evaluated *Cst3* mRNA (Figure S1B) and CST3 protein levels (Figures 1A–1D) in the brain and spinal cord of female and male mice before disease induction and at the peak of $MOG_{35–55}$-induced EAE. *Cst3* mRNA was observed to be constitutively expressed in the brain of naive female and male C57BL/6J animals (Figure S1B), and the protein level of CST3 was significantly augmented in the brain and spinal cord of mice with EAE (Figures 1A–1D); this expression did not differ according to the sex of mice examined (Figures 1A–1D). As such, EAE was deemed an appropriate model to study the function of CST3 in MS.

CST3 Enhances CNS Inflammation and Clinical Severity Selectively in Female Mice during EAE

To assess whether CST3 plays a role in the development of EAE, disease disability was monitored in *Cst3* null ($Cst3^{-/-}$) and *Cst3*-overexpressing (*Cst3*Tg) female and male mice immunized with $MOG_{35–55}$. Relative to their wild-type (WT) littermate counterparts, clinical signs of EAE were significantly attenuated in female $Cst3^{-/-}$ animals as compared to controls (Figure 1E; Table S2), while female *Cst3*Tg animals demonstrated an enhancement of clinical disability at peak disease (Figure 1G; Table S3). Although $Cst3^{-/-}$ males exhibited a slight delay in onset of EAE compared to WT counterparts, $Cst3^{-/-}$ males rapidly developed strong disability thereafter so that that there was no difference in clinical signs between WT and $Cst3^{-/-}$ male EAE animals from peak disease onward (Figure 1F). In alignment with these results, there were no differences in disease scores between EAE male *Cst3*Tg animals and their WT littermate controls (Figure 1H). Altogether, these results indicate that CST3 has a deleterious role in the C57BL/6J EAE model, but mainly in females. Notably, because the *Cst3*Tg animals developed severe clinical signs and high mortality with the standard immunization protocol, and because C57BL/6J WT mice normally display strong clinical disease with the full immunization regiment, we reduced the concentration of the $MOG_{35–55}$ and pertussis toxin for experiments using the *Cst3*Tg animals to allow for survival and to differentiate for any differences between the *Cst3*-overexpressing animals and their C57BL/6J WT counterparts.

Next, to evaluate whether the EAE clinical signs between female and male $Cst3^{-/-}$ EAE mice correlated with histopathological features, quantification of immune cell infiltrates and demyelination in EAE spinal cord was carried out at peak EAE using flow cytometry and histological staining. Although no differences were seen between male WT and male $Cst3^{-/-}$ EAE mice in the number of total $CD45^+$ cells or other immune cell subsets that infiltrated into the spinal cord by flow cytometry (Figure 2B), there were significantly fewer $CD45^+$ immune cells, $CD3^+$ and $CD4^+$ T cells, $CD11b^+CD45^{high}$ macrophages, $CD11b^+CD45^{med}$ microglia, and $CD11c^+$ DCs in the spinal cord of female $Cst3^{-/-}$ EAE mice compared to

their WT counterparts (Figure 2A); very few $CD8^+$, $B220^+$, and $Ly6G^+$ cells were present in the spinal cords of mice, regardless of genotype or sex. Consistent with these findings, histological analysis revealed a marked reduction in the number of immunopositive $CD45^+$ immune profiles in the spinal cord of female but not male *Cst3*$^{-/-}$ EAE animals as compared to sex-matched WT controls (Figures 2C and 2D). Similarly, in regard to demyelination, the area of myelin loss in spinal cord as revealed by eurochrome cyanine staining was markedly less in female *Cst3*$^{-/-}$ mice with EAE as compared to female WT EAE animals, whereas this histological characteristic was not different between male WT and male *Cst3*$^{-/-}$ EAE mice (Figures 2E and 2F).

IL-6 and IFN-γ Production by Spleen and Lymph Node Immune Cells Is Reduced during EAE in Female *Cst3*$^{-/-}$ Animals

To gain insights into the sex-dependent mechanism(s) of CST3 regulation of CNS inflammation, we examined the production of cytokines by immune cells ($CD45^+$ cells) in the spleen and draining lymph nodes, where immune cells are primed and circulate during EAE. First, the expression of cytokines (IL-2, IL-4, IL-6, IL-10, IL-12p40, IL-17A, granulocyte-macrophage colony-stimulating factor [GM-CSF], IFN-γ, tumor necrosis factor alpha [TNF-α]) was evaluated in lymph node and spleen cells by intracellular cytokine staining after immunization with $MOG_{35–55}$/complete Freund's adjuvant (CFA) (EAE) or CFA alone (Figures 3 and S2). As expected, we observed higher levels of expression of IL-2, IL-6, IL-12p40, IL-17A, IFN-γ, and TNF-α in total $CD45^+$ leukocytes in the draining lymph node and spleen of male and female WT EAE animals relative to CFA controls (Figures S2A, S2B, S2K, and S2L). However, while male EAE *Cst3*$^{-/-}$ $CD45^+$ cells showed an increased expression for these cytokines that is similar to that of their WT counterparts, the mean fluorescence intensity (MFI) for IL-6 and IFN-γ was significantly lower in $CD45^+$ cells isolated from the spleen or lymph nodes of female *Cst3*$^{-/-}$ EAE mice relative to the WT cohorts; IL-12p40, IL-17A, and TNF-α expression did not differ from that in controls (Figures S2A, S2B, S2K, and S2L). Only low levels of IL-4, IL-10, and GM-CSF were expressed by these cells, and this expression did not vary by mouse sex or genotype (Figures S2A, S2B, S2K, and S2L).

To gain insights into the cell source of the differential IFN-γ and IL-6 expression in female WT versus female *Cst3*$^{-/-}$ $CD45^+$ cells, we next analyzed cytokine production in specific immune cell populations ($CD4^+$, $CD8^+$, $CD11b^+$, $CD11c^+$, $B220^+$, and $Ly6G^+$). Compared to the female WT group, we found that IFN-γ MFI was significantly reduced in female *Cst3*$^{-/-}$ $CD4^+$ T cells in both the EAE lymph node (Figure 3A) and spleen (Figure 3G), whereas no difference in expression of this cytokine was evident in $CD8^+$ T cells in both organs (Figures S2E and S2O). Again, IFN-γ MFI did not differ between male WT and *Cst3*$^{-/-}$ counterparts (Figures 3B, 3H, S2F, and S2P). Although IL-2 and IL-17A expression was observed to be markedly increased in $CD4^+$ T cells during EAE, these levels did not differ between female or male WT and *Cst3*$^{-/-}$ mice in these studies (Figures 3A, 3B, 3G, and 3H).

With respect to IL-6, we noted significantly reduced expression of this cytokine compared to WT in $CD11b^+$ and $CD11c^+$ cells (Figures 3C, 3E, 3I, and 3K), but not in $B220^+$ or $Ly6G^+$

cells (Figures S2G, S2I, S2Q, and S2S) from female *Cst3*$^{-/-}$ mice. This was true for both the draining lymph nodes and spleen. Again, no difference in IL-6 expression was evident between male WT and *Cst3*$^{-/-}$ APCs during EAE (Figures 3D, 3F, 3J, 3L, S2H, S2J, S2R, and S2T).

To explore whether CST3 regulated MOG-specific IFN-γ and IL-6 secretion during EAE, we also isolated spleen and lymph node cells from pre-symptomatic female and male WT and *Cst3*$^{-/-}$ EAE mice; cultured these cells with increasing concentrations of $MOG_{35–55}$; and evaluated the secretion of IL-1β, IL-2, IL-4, IL-6, IL-10, IL-12p40, IL-17, IFN-γ, and TNF-α by ELISA. In EAE-derived splenocytes and lymph node cells, very low IL-4 and IL-10 secretion was detected, and while IL-1β, IL-2, IL-17, and TNF-α levels increased with $MOG_{35–55}$ stimulation for both female and male WT and *Cst3*$^{-/-}$ mice, the changes between WT and *Cst3*$^{-/-}$ were inconsistent; thus, no conclusions could be drawn (data not shown). However, in all experiments, the production of IFN-γ and IL-6 was significantly lower in splenocytes from female *Cst3*$^{-/-}$ EAE animals relative to female WT cells (Figures 4A and 4C). Although the production of IFN-γ and IL-6 by female *Cst3*$^{-/-}$ lymph node cells was also reduced relative to WT at certain $MOG_{35–55}$ concentrations, the differences were less striking than that seen in the spleen (Figures 4E and 4G); it is possible that the encephalitogenic ability of the lymph node cells declined in culture. Of note, however, IL-6 and IFN-γ levels did not differ between male WT and male *Cst3*$^{-/-}$ groups in either the spleen or lymph node (Figures 4B, 4D, 4F, and 4H). Altogether, these data reveal that CST3 expression promotes the expression of IL-6 (a prototypic APC cytokine) by $CD11b^+$ and $CD11c^+$ cells and IFN-γ (a prototypic Th1 cytokine) by $CD4^+$ T cells in female, but not male, mice during EAE. The specificity of CST3 in the regulation of IL-6 and IFN-γ is noteworthy, considering the pro-inflammatory role of these cytokines in EAE and MS, where administration of IFN-γ during the immunization phase for EAE promotes an earlier onset of the disease (Naves et al., 2013) while IL-6 is involved in the development of pathogenic Th1and Th17 cells (Petković and Castellano, 2016).

CST3 Mediates Sex-Dependent Effects on Th1 Cytokine Production in Female Mice via Effects in APCs

Because IFN-γ is a prototypic Th1 $CD4^+$ T cell cytokine, we postulated that regulation of this cytokine by CST3 may occur via a $CD4^+$ T cell-intrinsic mechanism. To test this idea, $CD4^+$ T cells from naive male and female WT and *Cst3*$^{-/-}$ mice were isolated and stimulated *in vitro* with anti-CD3/anti-CD28 and secretion of IFN-γ evaluated by ELISA. We observed that IFN-γ production by *Cst3*$^{-/-}$ $CD4^+$ T cells was reduced compared to WT $CD4^+$ T cells, but interestingly, this occurred in both sexes (Figures 5A and 5B). These results indicate that CST3 does play a role in the regulation of T cell IFN-γ production, but that CST3 functioning in T cells did not underlie the sex-dependent effect of CST3 on MOG-specific Th1 responses (Figures 3 and 4) or clinical disability seen during EAE (Figures 1E–1H).

Since the difference between the splenocyte experiment (Figures 4A and 4B) and the $CD4^+$ T cell assay (Figures 5A and 5B) was the presence of APCs in the former, and that IL-6, an APC cytokine, was altered in female but not male EAE $CD11b^+$ and $CD11c^+$ lymph

node and spleen cells as well as splenocytes (Figures 3 and 4), we hypothesized that IL-6 and IFN-γ regulation by CST3 in female mice may be mediated through activities in APCs. Indeed, when female *Cst3*$^{-/-}$ CD4^{+} T cells were co-cultured with female splenocytes from *Cst3*$^{-/-}$ EAE animals (as a source of APCs), the levels of IFN-γ were much lower than those in the female WT T cell + WT splenocyte co-cultures (Figure 5C), whereas there was no discernible difference in production of this cytokine between the male WT and *Cst3*$^{-/-}$ co-cultures (Figure 5D). Furthermore, switching the genotype of the APC modulated the IFN-γ production; that is, lowered secretion of IFN-γ was noted when female WT CD4^{+} T cells were cultured with female *Cst3*$^{-/-}$ splenocytes, while an augmentation in IFN-γ levels was evident when female *Cst3*$^{-/-}$ CD4^{+} T cells were cultured with female WT splenocytes (Figure 5C). For male cells, however, switching the genotype of the APC did not alter IFN-γ secretion by male WT or *Cst3*$^{-/-}$ CD4^{+} T cells (Figure 5D).

Since CD11b^{+} DCs expressCST3 (Figure S3A) and are the critical cells mediating Th cell priming (Lehmann et al., 2017) and Th cell reactivation in the CNS during EAE (Bailey et al., 2007), we also evaluated the potential of purified WT and *Cst3*$^{-/-}$ spleen CD11b^{+} cells (derived from EAE mice) to secrete IL-6 or to support IFN-γ production by $MOG_{35–55}$-specific Th cells. We found that the production of IL-6 by female *Cst3*$^{-/-}$ CD11b^{+} cells was reduced relative to female WT cells upon stimulation with LPS, while no difference in secretion of this cytokine wasevident between male WT and *Cst3*$^{-/-}$ CD11b^{+} cells (Figures 5E and 5F). Similar results were observed in cultures of peritoneal macrophages (Figures S3B–S3E).

Next, we evaluated whether the *Cst3*$^{-/-}$ genotype in CD11b^{+} cells could impart changes in IFN-γ production by CD4^{+} T cells. We measured for IFN-γ, since this cytokine was one of the two (IL-6 being the other) altered in female *Cst3*$^{-/-}$ EAE lymph node-derived (Figure 3A) and spleen-derived (Figure 3G) CD4^{+} T cells and splenocytes (Figure 4A). For this experiment, spleen-derived CD11b^{+} cells from EAE mice (Figures 5G, 5H, S4E, and S4F) or, alternatively, bone-marrow-derived macrophages (BMDMs) from naive mice of the various groups (Figures S3C and S3D) were co-cultured with sex-matched MOG-reactive CD4^{+} T cells derived either from mice with EAE (Figures 5G, 5H, S4C, and S4D) or from 2D2 MOG T cell receptor transgenic mice (Figures S4E and S4F). We observed that female CD4^{+} T cells from *Cst3*$^{-/-}$ EAE animals, when grown with female *Cst3*$^{-/-}$ spleen CD11b^{+} cells, exhibited markedly reduced MOG-elicited IFN-γ production as compared to those cultured with WT CD11b^{+} cells (Figure 5G). Again, the T cell production of IFN-γ was modulated by alternating the genotype of the CD11b^{+} cell (Figure 5G). That is, IFN-γ production was reduced when female WT EAE CD4^{+} T cells were grown with female EAE *Cst3*$^{-/-}$ CD11b^{+} cells, and vice versa, IFN-γ secretion was enhanced when CD4^{+} T cells from female *Cst3* null EAE mice were co-cultured with female WT EAE APCs. For male cells, however, no difference in IFN-γ production was observed when male WT EAE CD4^{+} T cells were co-cultured with male EAE CD11b^{+} cells from either the syngeneic or the alternate genotypes (Figure 5H). Similar results were observed in experiments of MOG-reactive CD4^{+} T cells grown with BMDMs (Figures S4C and S4D) or when 2D2 CD4^{+} T cells were co-cultured with spleen-derived CD11b^{+} cells from EAE mice (Figures S4E and S4F). These data indicate that CST3 has a more prominent role in regulating IL-6 production and APC function in females and that this role is shared among a number of

CD11b$^+$ subsets. Our results further suggest that CST3 expression in APCs likely accounted for the sex-dependent effect of CST3 on MOG-specific Th1 cytokine responses and EAE development.

Antigen Presentation Markers on Female APCs Are Regulated by CST3 during EAE

We next sought to decipher the molecular mechanism(s) by which CST3 regulates APC function in female animals. Since CD4$^+$ T cell activation was influenced by CST3 in CD11b$^+$ cells, it suggested that the antigen-presenting ability of APCs may be impacted by CST3. Therefore, we assessed for the protein level of key molecules that are involved in the processing and loading of antigens onto MHC II (LC3I and LC3II), antigen presentation, and T cell co-stimulation (MHC II, CD80, and CD86) (Figure S5). As such, we compared the levels of these proteins in CD11b$^+$ cells isolated from naive mice or animals immunized with $MOG_{35–55}$ + CFA (EAE) or CFA alone. As expected, male and female WT CD11b$^+$ cells from EAE mice exhibited significantly augmented expression of CD80, CD86, MHC II, LC3I, and LC3II (active form of LC3) relative to WT cells from naive mice (Figures 6A and 6B). An upregulation of some of these proteins was also seen in the female WT CFA group (Figure 6A), with male CFA WT APCs augmenting their levels of all the antigen-processing and presentation factors, similar to that of WT EAE cells (Figure 6B). Of note, however, female *Cst3*$^{-/-}$ mice did not exhibit upregulated expression of these markers in CD11b$^+$ cells in either the CFA group or the EAE group, whereas this same defect was not apparent in males (Figures 6A and 6B).

These data were corroborated by flow-cytometric analysis of female and male WT and *Cst3*$^{-/-}$ naive, CFA, and EAE CD11b$^+$, CD11c$^+$, and B220$^+$ cells, as well as RNA-sequencing (RNA-seq) analysis of female and male WT and *Cst3*$^{-/-}$ EAE CD11b$^+$ cells. Similar to the western blot data, we found by flow cytometry that the MFI for CD80, CD86, and MHC II was increased as expected in female and male EAE CD11b$^+$, CD11c$^+$, and B220$^+$ cells relative to WT naive animals (Figures 6C–6H and S6). Also, in WT CFA female and male CD11b$^+$, CD11c$^+$, and B220$^+$ cells, CD86 expression was comparable to that found in the EAE group (Figures 6E, 6F, and S6C) with MHC II MFIs in female and male WT CFA CD11c$^+$ and B220$^+$ cells similar to those of their EAE counterparts (Figures 6H and S6D). Of note, CD80, CD86, and MHC II MFIs were markedly lower in female *Cst3*$^{-/-}$ CD11b$^+$ cells compared to those in WT counterparts during EAE (Figures 6C, 6E, and 6G). A smaller but significant reduction was also seen for MHC II expression in CD11c$^+$ cells from female CFA and female EAE *Cst3*$^{-/-}$ mice as compared to female WT controls (Figure 6H). Again, there was no difference in the expression of these proteins between male WT or *Cst3*$^{-/-}$ groups for any of these cell populations (Figures 6C–6H and S6).

Our RNA-seq data also revealed that LC3B and CD80 in female EAE *Cst3* null cells were overwhelmingly present in immune-modulation functional pathways that were decreased compared to the male cohort (Figures S7A and S7B; Table S4). These findings imply that CST3 plays a role in promoting an appropriate molecular response needed for the maturation or antigen processing, loading, and presentation by APCs in female mice during EAE. To provide more direct evidence for this assertion, we transfected *Cst3* into female *Cst3*$^{-/-}$ BMDMs stimulated with or without LPS. This resulted in a restoration of CD80, CD86,

MHC II, and LC3I/II expression upon LPS stimulation relative to control transfected cells (Figure S7C).

CST3's Sex-Dependent Function in EAE Is Regulated by Gonadal Hormones

Finally, we were interested in understanding why CST3 modulated APC function and EAE disease differently in females and males. Our data did not reveal a sex difference in the expression of CST3 in either the CNS (Figures 1A–1D and S1) or $CD11b^+$ cells (Figure S3A), suggesting that this protein was not under the direct control of sex hormones. However, the possibility remained that CST3 was involved in a pathway that was regulated by sex hormones. To test this idea, we investigated whether CST3's effects in EAE could be modulated by switching the hormonal environment of male and female mice. To this end, EAE was induced in female WT and *Cst3*$^{-/-}$ mice that were ovariectomized and administered testosterone or placebo or in male WT and *Cst3*$^{-/-}$ animals that were castrated and provided with estradiol + progesterone (E/P) or placebo. Ovariectomy or castration with or without placebo did not alter the course of EAE in WT female and male animals, respectively (Figures 7A and 7B; Tables S5 and S6). Of note, however, the disease course of ovariectomized + testosterone-administered female *Cst3*$^{-/-}$ animals shifted to a male-like clinical phenotype whereby there was no difference in disability between WT and *Cst3*$^{-/-}$ EAE mice (Figure 7A; Table S5). The reverse was seen in castrated male animals administered E/P, where male *Cst3*$^{-/-}$ animals that normally showed no difference in clinical disability as compared to male WT controls (Figure 1F) now demonstrated a significant amelioration of disease (Figure 7B; Table S6). This acquisition of sensitivity of EAE to the effects of CST3 deficiency in the castrated male + E/P *Cst3*$^{-/-}$ cohort did appear to relate to a reduced ability of this group's $CD11b^+$ cells to activate $CD4^+$ T cells. When spleen $CD11b^+$ cells were isolated from male WT and *Cst3*$^{-/-}$ mice with these hormone treatments and co-cultured with MOG-reactive 2D2 $CD4^+$ T cells, a very low level of IFN-γ was secreted by the 2D2 $CD4^+$ T cells cultured with castrated male + E/P *Cst3*$^{-/-}$ $CD11b^+$ cells as compared to the castrated WT male + E/P group (Figure S8A).

We also evaluated whether the sex-dependent regulation of IL-6 production by CST3 in splenic $CD11b^+$ cells could be modulated by *in vitro* treatment with sex hormones. For these studies, $CD11b^+$ cells from either naive (Figures S8B–S8Q) or EAE (Figures 7C–7R) female and male mice were stimulated with LPS with or without estradiol or dihydroxytestosterone (DHT); and IL-1β, IL-6, IL-12p40, and TNF-α secretion was measured by ELISA. We did note a significant upregulation of IL-1β, IL-12p40, and TNF-α in response to LPS, but no differences were evident in cytokine production between WT and *Cst3*$^{-/-}$ cells from either sex or in response to estradiol and DHT application (Figures 7C–7F, 7K–7R, S8B–S8E, and S8J–S8Q). However, we did observe that, overall, estradiol did repress, whereas testosterone tended to increase, the secretion of IL-6 by $CD11b^+$ cells from naive or EAE groups; however, the *in vitro* hormone treatment could not reveal an effect of CST3 deficiency on IL-6 in male cells or repress an effect of CST3 deficiency in female cells (Figures 7G–7J and S8F–S8I). This suggested that the effect of sex hormones on the CST3 effect on IL-6 is more complex and cannot be appropriately modeled using an *in vitro* system. Nonetheless, these findings suggested a role for gonadal hormones in driving the sex dependence of CST3 effects on Th1 responses and EAE severity.

DISCUSSION

In this study, we sought to clarify the function of CST3 whose mRNA and protein levels are increased in the brains of MS patients and the CNS of EAE mice, respectively. Using the C57BL/6J EAE model, we found that CST3 plays a sex-dependent detrimental role in EAE, whereupon CST3 has a selective effect in females in promoting activation of APCs and Th1 responses leading to more severe EAE disability in this sex.

The main finding of our study was that CST3 regulated antigen presentation and co-stimulation machinery as well as IL-6 production by $CD11b^+$ cells in female mice. These findings of CST3 in APCs do corroborate previous findings by other groups. For example, Frendéus et al., 2009 showed that treating WT and *Cst3* null macrophages with CST3 and IFN-γ led to stimulation of the IFN-γ-mediated nuclear factor κB (NF-κB) P65 pathway to result in inducible nitric oxide synthase (iNOS) and TNF-α production, while downregulating IL-10 expression. CST3 also plays important roles in the maturation of monocytes and DCs, as well as regulating the function of cathepsins and invariant chain processing in macrophages and DCs (El-Sukkari et al., 2003; Pierre and Mellman, 1998; Rodriguez-Franco et al., 2012; Warfel et al., 1987) that can impact antigen presentation. In our studies, we found that CD80, CD86, and MHC II expression levels were reduced in female $Cst3^{-/-}$ EAE $CD11b^+$ cells as compared to levels in female WT or male groups. This impacted the ability of MOG-reactive $CD4^+$ T cells to make the prototypic effector cytokine, IFN-γ, *in vitro* and *in vivo*. It is likely that this decrease in APC activation and Th1 responses was also the main contributor to why fewer immune cells infiltrated the CNS in the female $Cst3^{-/-}$ EAE mice. Indeed, CD80 and CD86 have been shown to have pivotal roles in initiating inflammation in EAE; their inhibition reduces the disease (Chang et al., 1999; Cross et al., 1995). Although Th17 cells are also important for EAE development, IFN-γ production by Th cells is important in regulating the initial entry of these cells into the CNS (O'Connor et al., 2008). It is also noteworthy that binding of CD28 to CD80/86 induces the production of IL-6 (Orabona et al., 2004), the only APC cytokine we found altered in female versus male $Cst3^{-/-}$ $CD11b^+$ and $CD11c^+$ cells. In apparent discordance with our data, a study by Bäcklund et al., 2011 showed significant upregulation of CD80, CD86, and MHC II in *Cst3*KO male DCs in CIA. The main difference with their study is that only male mice were included in their experiments. In addition, *Cst3* and WT colonies were on a different genetic background, which may contribute to microbiota drift in the $Cst3^{-/-}$ colony. Nonetheless, coinciding with this past study, we did observe a significant enhancement in CD86, but not CD80 or MHC II, expression in male $Cst3^{-/-}$ $CD11b^+$ cells relative to the WT mice in the EAE group.

It is notable that this sex-dependent regulation of APC function by CST3 was more prominent in $CD11b^+$ cells than in $CD11c^+$ cells; MHC II and IL-6, but not CD80 and CD86, expression was sensitive to CST3 regulation in $CD11c^+$ cells, whereas all of these proteins were sensitive to CST3 regulation in $CD11b^+$ cells. However, our co-culture experiments did use magnetically enriched $CD11b^+$ cells, which would also include $CD11b^+$ $CD11c^+$ DCs. $CD11b^+CD11c^+$ DCs are the subset most responsible for priming $CD4^+$ T cells *in vivo* (Dudziak et al., 2007). Therefore, it is likely that CST3 functioning in both

$CD11c^+$ and $CD11b^+$ cells contributed to the enhanced Th1 responses and immune cell infiltration seen in female WT versus *Cst3*$^{-/-}$ mice during EAE.

In addition to expression of MHC II and co-stimulatory molecules, antigens have to be properly cleaved and then loaded onto MHC II for antigen presentation to occur. Autophagy is a key mechanism in the cleavage of antigens and their transfer to MHC II (Patterson and Mintern, 2012; Wang and Muller, 2015). In this regard, previous studies have reported that CST3 promotes autophagy activation through the inhibition of mammalian target of rapamycin (mTOR) (Tizon et al., 2010a), an inhibitor of autophagy. We found here that CST3 also regulated the expression of LC3A/BII in female $CD11b^+$ cells, which is an essential end product of autophagy that is involved in antigen processing and antigen loading in the autophagolysosome. Our data thus imply that antigen presentation would be disrupted, since antigen processing and loading onto MHC II would be inadequate in female *Cst3*$^{-/-}$ cells. This observation was recently supported in macrophages during atherosclerosis where absence of CST3 in macrophages led to a dysfunction of autophagy in these cells and, subsequently, to their apoptosis (Li et al., 2016).

Sex chromosomes and sex hormones have been implicated in driving the sex difference seen in MS and among the SJL/J, ASW, NZW, B10.PL, and PL/J strains of mice with EAE (Papenfuss et al., 2004; Ramien et al., 2016). C57BL/6 mice do not typically display a sex difference in EAE disability (Voskuhl and Palaszynski, 2001), which we also observed. Although we observed higher IFN-γ production by female MOG-activated lymph node or spleen cells in EAE (Figure 4), a feature also reported by previous groups (Dunn et al., 2007; Palaszynski et al., 2005), we did not observe consistent sex differences in IFN-γ production or other immune parameters in our *in vitro* studies, underscoring that the C57BL6/J mouse may not be the best mouse strain to model the sex differences that occur in MS. Nonetheless, by comparing the phenotypes of male and female WT and *Cst3*$^{-/-}$ mice, our studies did reveal a striking sex difference in the impact of CST3 on the expression of IL-6 and key molecules involved in the antigen-presenting and co-stimulatory machinery of APCs, where CST3 enhanced these immune parameters selectively in the female mice. The sex dependence of CST3 function was not due to sex differences in expression of this protein. To understand why knocking out or overexpressing CST3 modulated EAE in female mice, but not male mice, we designed experiments to shift the hormone environment of mice. We observed that imparting a male hormone environment to the female mice reduced the impact of CST3 deficiency in EAE, whereas imposition of a female hormone environment in the males revealed CST3 function in the males. We further found that the CST3 dependence in EAE correlated with the ability of isolated $CD11b^+$ T cells to prime $CD4^+$ T cells *ex vivo*. It still remains unclear how these hormone shifts can modulate these effects of CST3 on APC function. We speculate that there may be functional redundancy between CST3 and another protein (or proteins), “X,” that is expressed at higher levels in males than in females and can, therefore, compensate for the lack of CST3 function in male APCs more than female APCs. That is, when CST3 is knocked out, this protein can compensate for the lack of CST3 function in male, but not female, APCs. If this is the case, our data suggest that protein “X” is turned off by female sex hormones. A future study will aim to understand whether and how female sex hormones impact CST3 function.

Finally, CST3 is expressed not only by peripheral APCs but also by CNS cells such as neurons, astrocytes, and microglia (Aronica et al., 2001; Solem et al., 1990; Zucker-Franklin et al., 1987). Since microglia and astrocytes can contribute to leukocyte trafficking via cytokine and chemokine secretion—and, possibly, T cell reactivation and T cell differentiation in EAE/MS (Beurel et al., 2014; Falsig et al., 2006; Giraud et al., 2010; Hayashi et al., 1995; Wang et al., 2013; Xie et al., 2015)—it is possible that CST3 expression in microglia and astrocytes may have also contributed to the EAE effects that we observed in the *Cst3*$^{-/-}$ mice. Future work using conditional null *Cst3* animals could evaluate whether CST3 in microglia and astrocytes impact EAE development and the sex-dependent effect we observe with the *Cst3*$^{-/-}$ mice.

Altogether, we have discovered that CST3 has a sex-dependent role in EAE development in C57BL/6J mice. We show that, in females, CST3 drives the activation and antigen-presenting ability of APCs to subsequently promote CD4^{+} IFN-γ production and CNS autoimmunity.

STAR★METHODS

RESOURCE AVAILABILITY

Lead Contact—Further information and requests for resources and reagents should be directed to and will be fulfilled by the Lead Contact, Shalina S. Ousman (sousman@ucalgary.ca).

Material Availability—This study did not generate new unique reagents.

Data and Code Availability—The RNA Sequencing dataset generated during this study are available from the NCBI GEO Repository under accession number GSE157624 (https://www.ncbi.nlm.nih.gov/geo/query/acc.cgi?acc=GSE157624).

EXPERIMENTAL MODEL AND SUBJECT DETAILS

Mice—Cystatin C null (*Cst3*$^{-/-}$) and *Cst3* overexpressing (*Cst3*Tg) mice were generated by Dr. Anders Grubb (Lund University) (Huh et al., 1999) and Dr. Efrat Levy (New York University) (Pawlik et al., 2004) respectively while 2D2 (C57BL/6-Tg(Tcra2D2,Tcrb2D2)1Kuch/J) mice were obtained from Jackson laboratories. The *Cst3*$^{-/-}$, *Cst3*Tg and 2D2 mice were maintained on a C57BL/6J background with controls consisting of WT littermates. Animals were housed at the University of Calgary under specific pathogen-free conditions with a constant 12h light/12h dark cycle and *ad libitum* access to food and water. All animal studies were conducted in accordance with Canadian Council on Animal Care guidelines.

Human brain samples—Fresh, frozen adult MS and normal brain samples were obtained from the United Kingdom Multiple Sclerosis Society Tissue Bank (Ethics ID: REB14–0945, University of Calgary). The characteristics of the tissues including sex, age, type of MS, lesion type and brain area sampled are displayed in Table S1.

Active EAE—Eight to 12-week-old female and male *Cst3*$^{-/-}$ and C57BL/6J WT littermates were immunized subcutaneously with 100μg myelin oligodendrocyte glycoprotein 35–55 ($MOG_{35–55}$) (Stanford Pan Facility) mixed in a 1:1 emulsion with complete Freund's adjuvant that contained 4mg/ml *Mycobacterium Tuberculosis* H37Ra (Fisher Scientific). Animals were also administered 400ng of *Bordetella Pertussis* toxin (PTX) (List Biological Laboratories Inc.) intravenously on days 0 and 2 post-immunization. Since the *Cst3*Tg animals developed severe clinical signs and displayed high mortality compared to their littermate C57BL/6J controls with the standard immunization protocol described above, we reduced the concentration of the immunization emulsion reagents for *Cst3*Tg animals in order to differentiate differences with their WT counterparts and to reduce the mortality rate - death is not an allowable end-point for our Animal Care Council. *Cst3*Tg animals were thus immunized with 50μg $MOG_{35–55}$ + 1mg/ml *Mycobacterium Tuberculosis* and 200ng PTX. Mice were scored on a 5 point disability scale where 0 = normal, 1 = limp tail, 2 = weak hindlimbs, 3 = complete hindlimb paralysis, 4 = complete hindlimb paralysis with some forelimb weakness, and 5 = moribund/death. Please note that although the clinical signs are milder for the *Cst3*Tg and their littermate controls, both genotypes still develop the EAE disability profile that is characteristic for C57BL/6J mice.

Immune cell isolation and activation

Splenocytes and lymph node cells: Spleens and axial and inguinal lymph nodes were crushed through a 70μm mesh cell strainer followed by lysing of spleen red blood cells with Ammonium-Chloride-Potassium (ACK) lysis buffer. 500,000 cells/well were grown in complete Roswell Park Memorial Institute (RPMI) media [RPMI (Thermo Fisher Scientific, 11875093), 10% heat-inactivated fetal bovine serum (FBS) (Thermo Fisher), 100U/ml penicillin/streptomycin (Thermo Fisher Scientific, 10378016), 2mM L-glutamine (Thermo Fisher Scientific, 25030081), 1% sodium pyruvate (Thermo Fisher Scientific, 11360070), 1% non-essential amino acids (Thermo Fisher Scientific, 11140050)] for 5 days at 37°C and 5% CO_2 with 2.5, 5 and 10 μg/well $MOG_{35–55}$.

$CD4^+$ and $CD11b^+$ cells—Following red blood lysis with ACK lysis buffer, $CD4^+$ T cells (Miltenyi Biotec) and $CD11b^+$ cells (Miltenyi Biotec) were isolated by positive selection from splenocytes. For anti-CD3/anti-CD28 stimulation, 100,000 $CD4^+$ T cells/well were cultured for 3 days in complete RPMI media in round bottom plates coated with 0.1, 0.5 and 1μg/ml of purified hamster anti-mouse CD3 (BD) and anti-mouse CD28 (BD) (see Reagent or Resource in the Key Resources Table).

Peritoneal macrophages—Eight to twelve-week-old mice were injected intraperitoneally (i.p.) with 3ml of thioglycollate broth (BD Bioscience). After 3 days, the mice were euthanized and injected i.p. with 5ml of cold Dulbecco's Modified Eagle Medium (DMEM) (Thermo Fisher Scientific). The peritoneal cavity DMEM solution was collected and centrifuged at 1400rpm for 10 min at 4°C. The pellet was resuspended in DMEM media containing 1% sodium pyruvate, 1% glutamine, and 1% penicillin/streptomycin. 500,000 cells/well were plated in 24 well plates and stimulated with 100ng/ml LPS for 24 hours at 37°C in 5% CO_2.

BMDMs—Hind limbs were removed from naive mice and muscles extracted from the bones. Bone marrow was flushed from the femurs and tibias using cold sterile DMEM (Thermo Fisher Scientific). Cells were counted and centrifuged at 1200rpm for 10 minutes at 4°C. Bone marrow cells were incubated with DMEM supplemented with 10% charcoal stripped FBS (Thermo Fisher Scientific), 45% L929-conditioned media, 1% glutamine, and 1% penicillin/streptomycin for 10 days followed by an 18h incubation with 100U/ml of recombinant mouse (rm)-IFN-γ (Thermo Fisher Scientific) (see Reagent or Resource in the Key Resources Table). Purity of BMDMs was verified by flow cytometry using $CD45^+$ and $CD11b^+$ staining (Figure S4A).

T cell/APC co-culture—Irradiated (1400rads) splenocytes, spleen-derived $CD11b^+$ cells or BMDMs were plated in a 5:1 ratio (250,000/50,000) with $CD4^+$ T cells in complete RPMI media for 5 days at 37°C and 5% CO_2 in the presence or absence of 2.5, 5 and 10 μg/ml $MOG_{35–55}$.

$CD11b^+$ cells and sex hormones—250,000 spleen-derived $CD11b^+$ cells/well were cultured with 1nM estradiol (Sigma) or 1nM DHT (Sigma) for 24h followed by LPS (100ng/ml) stimulation for 20 hours; see Reagent or Resource in the Key Resources Table.

Gonadectomy and hormone administration (Liva and Voskuhl, 2001; Matejuk et al., 2005; Ziehn et al., 2012)—Mice were anaesthetized with 200mg/kg:10mg/kg ketamine/xylazine. Ovaries were removed in four-week-old anaesthetized female animals by making one 5mm incision on the medial dorsal site, followed by two small bilateral peritoneal incisions halfway between the front and hindlimbs. The ovaries were localized, pulled from the incision site, and excised. The incision was closed using single interrupted sutures. For hormone replacement, ovariectomised animals were implanted subcutaneously two weeks later with a 60d release Alzet pump containing 5mg testosterone (4-ANDROSTEN-17β-OL-3-ONE, Steraloids Inc.) (0.083mg/day released) diluted in 10.9% ethanol in saline. Placebo consisted of 10.9% ethanol in saline. The animals were induced with EAE two weeks later at 8 weeks of age.

Male mice were castrated at four weeks of age. One 5mm incision was made on the caudal ventral site, followed by one small peritoneal incision. Testes were pulled from the incision site and removed by cauterization (Bovie Medical Corporation). The incision was then closed using single interrupted sutures. For hormone replacement, a 90d release 0.5mg 17β-estradiol/10mg progesterone or placebo pellet (Innovative Research of America) was implanted subcutaneously at the time of castration; see Reagent or Resource in the Key Resources Table. Animals were immunized for EAE at 8 weeks of age.

METHOD DETAILS

Protein isolation and western blotting—Total protein was isolated from cells and tissues using 50mM Tris–hydrochloride (HCl) pH 7.4, 1% NP-40, 10% glycerol, 1mM ethyl-enediaminetetraacetic, 1mM sodium vanadate, 1mM sodium fluoride, 1mM dithiothreitol, 4.5mM sodium pyrophosphate, 10mM beta-glycerophosphate, and a protease inhibitor cocktail tablet (Roche Diagnostics). After centrifugation at 14,000 rpm at 4°C

for 20–30 min, supernatants were collected and protein content determined at 560nm absorption. Fifty micrograms of protein was suspended in two volumes of double-strength sodium dodecyl sulfate (SDS) sample buffer (Bio-Rad Laboratories) and subjected to 5%–15% gradient SDS–polyacrylamide gel electrophoresis. Proteins were transferred unto polyvinylidene fluoride membranes and blocked with 5% non-fat dried milk in Tris–HCl-buffered saline (TBS) containing 0.05% Tween-20. Membranes were immunoblotted overnight at 4°C with the following primary antibodies: rat anti-mouse Cystatin C (1:100, R&D Systems), rabbit anti-mouse CD86 (1:2000, Abcam), rat anti-mouse CD80 (1:400, R&D), rabbit anti-mouse MHC class II (1:1000, Abcam), rabbit anti-mouse LC3A/B (1:1000, Cell Signaling), or rabbit anti-mouse β-actin (1:1000, Sigma); see Reagent or Resource in the Key Resources Table. Primary antibodies were visualized using 1:5000 horseradish peroxidase-conjugated donkey anti-rabbit (GE Healthcare) or goat anti-rat (Cell Signaling) followed by chemiluminescence detection using an ECL kit (Pierce).

Immunohistochemistry—Mice were sacrificed by carbon dioxide overdose and perfused with 4% paraformaldehyde (PFA). Brains and spinal cords were post-fixed in 4% PFA for 24h, and then cryoprotected in 30% sucrose solution for 2 days before being frozen in optimal cutting temperature compound. Cross, longitudinal and coronal sections of 10 μm thickness were blocked with phosphate buffered saline (PBS) containing 0.1% Triton X-100 for 1 hour. Sections were then incubated overnight at 4°C with rat anti-mouse CD45 antibody (BD, 1:1000). Bound antibody was detected with anti-rat 488 secondary Ab (Thermo Fisher Scientific) at a 1:200 dilution while DAPI (Thermo Fisher Scientific, 1:2000) incubation for 10 minutes at room temperature allowed for nuclear identification.

Eriochrome cyanine myelin staining—Frozen 4% PFA-perfused spinal cords were sectioned at 10μm and dried at room temperature for 30 minutes. Sections were placed in acetone for 10 minutes, briefly rinsed in distilled water (dH_2O) and stained with 5% ferric ammonium sulfate (stains myelin blue) at room temperature for 10 minutes followed by five brief rinses in dH_2O. Tissues were decolorized in 0.1% NH_4 and placed in a mixture of 1% borax and 1.25% potassium ferricyanide (nuclei: pink) at room temperature for 1 minute, rinsed five times in dH_2O, dehydrated through graded ethanol solutions (1 min each in 70, 90, 95, and 100% ethanol and citrosol) and coverslipped using the mounting medium, Xylene (Fisher Scientific).

ELISA

Cytokines were measured in the supernatants of cultured cells at peak production using anti-mouse ELISA kits according to the manufacturer's instructions: 48h: IL-1β (BD), IL-2 (BD), IL-6 (BD), IL-12p40 (BD); 72h: IFN-γ (BD), TNF-α (R&D); 120h: IL-4 (BD), IL-10 (BD), IL-17 (R&D); see Reagent or Resource Table.

RNA isolation, RNA Deep Sequencing and RNASeq bioinformatics—$CD11b^+$ cells from d7 EAE female and male WT and *Cst3*$^{-/-}$ spleens were isolated by positive selection (Miltenyi Biotec) and RNA retrieved with an RNeasy Mini Kit (QIAGEN). Samples with an RNA integrity number greater than 8 were subjected to Deep Sequencing and each sample is from an individual mouse. All samples were subjected to reverse

transcription and Multiple Displacement Amplification with REPLI-g SensiPhi DNA Polymerase and oligo-dT primers as per the QIAGEN REPLI-g Single Cell RNA Library preparation kit and the manufacturer's protocol. Libraries were prepared using the QIAGEN GeneRead Adaptor I Set A 12-plex index adapters as per the REPLI-g single cell RNA library prep kit's protocol and subjected to on-board cluster formation and sequencing on an Illumina NextSeq 500 sequencer with a high-output v2 75 cycle sequencing kit as per the standard Illumina protocols; see Reagent or Resource in the Key Resources Table. After sequencing, the bcl data was converted to fastq data files using the Illumina BCL2FASTQ utility. Alignment was performed using bwa 0.7.12 in "mem" alignment mode against mm10 reference genome with default parameters. Output was imported into Ingenuity Pathway Analysis software for physiological function analysis.

RNA *in situ* hybridization—RNA *in situ* hybridization was performed as previously described (Touahri et al., 2015). Briefly, digoxygenin labeled RNA riboprobes for *Cst3* (cDNA Image clone ID: 3593373) were made using T7 (Invitrogen, for anti-sense probe; Restriction Enzyme: SalI) and SP6 (Biolabs, for negative control sense probe; Restriction Enzyme: Not1) RNA polymerases and digRNA labeling mix following the manufacturer's (Roche) protocol. RNA *in situ* hybridization was performed on 10μm sections collected on SuperFrost Plus slides (Thermo Scientific). Sections were hybridized with sense and anti-sense *Cst3* probes and incubated overnight at 65°C. Sections were then blocked (2% blocking reagent; Roche, made up in 10% normal horse serum) for 60 mins at room temperature, incubated overnight with anti-dig alkaline phosphatase antibody (Roche), and then stained with an NTMT (100 mM NaCl, 50 mM MgCl, 100 mM Tris pH 9.5, Tween 20) - levamisole solution containing NBT-BCIP (Roche) substrate. Sections were mounted post-staining using Permount Toluene solution (Fisher Scientific).

Fluorescence-activated cell sorting (FACS)—$0.5–1\times10^6$ primary splenocytes and lymph node cells and BMDMs were blocked with purified rat anti-mouse CD16/CD32 (BD Biosciences) at room temperature and incubated with various combinations of the following BD Biosciences fluorescently tagged anti-mouse antibodies for surface labeling at a concentration of 2.5% in the dark for 30 minutes at 4°C: APC-Cy7-conjugated CD45, APC-conjugated CD45, PerCP-conjugated CD45, BV711-conjugated CD3, FITC-conjugated CD3, APC-conjugated CD3e, PerCP-conjugated CD4, BV786-conjugated CD4, FITC-conjugated CD4, PE-conjugated CD8, BV650-conjugated CD8, FITC-conjugated CD11b, BV650-conjugated CD11b, BV421-conjugated CD11b, APC-conjugated CD11b, APC-conjugated CD11c, BV510-conjugated CD11c, Alexa700-conjugated CD11c, BV786-conjugated B220, FITC-conjugated B220, BV421-conjugated B220, PerCP5.5-conjugated Ly6G, FITC-conjugated Ly6G, PE-conjugated CD80, PE-Cy7-conjugated CD86, PerCP5.5-conjugated MHC II (CD80, CD86, MHC II gating is shown in Figure S6A). For phenotyping of the 2D2 mice, peripheral blood mononuclear cells were stained with FITC rat anti-mouse Vα 3.2 TCR (BD, 553219) or PE rat anti-mouse Vβ 11 T Cell (BD).

For cytokine analysis by intracellular flow cytometry, spleen and lymph node cells were processed according to the instructions for the Cytofix/Cytoperm Plus Fixation/ Permeabilization Kit from BD Biosciences. Briefly, spleen and lymph node cells from

female and male CFA- and EAE-immunized WT and *Cst3*$^{-/-}$ mice were isolated at day 6 post-immunization, stimulated *in vitro* with 10μg/ml $MOG_{35–55}$ for 15h and GolgiStop or GolgiPlug added in the last 4h. GolgiStop was used for IL-2, IL-4, IL-10, IL-17 and IFN-γ while GolgiPlug was used for IL-6, IL-12p40, GM-CSF and TNF-α. Cells were then labeled for cell surface markers above and the following cytokines: AF488-conjugated IL-2, PE-conjugated IFN-γ, AF647-conjugated IL-4, BV786-conjugated IL-17, BV421-conjugated IL-10, BV421-conjugated GM-CSF, BV711-conjugated TNF, FITC-conjugated IL-12p40, APC-conjugated IL-6; see Reagent or Resource in the Key Resources Table. An Attune acoustic or LSR II cytometer was used for acquiring cells and data analyzed with FlowJo 9.9.4. All experiments were performed on individual animals with each group consisting of 3–5 mice.

***Cst3* lentiviral packaging and transduction of primary BMDMs—**Total RNA was purified from a C57BL/6J whole mouse brain using the RNeasy lipid tissue mini kit (QIAGEN) according to manufacturer's instructions and converted to cDNA using the superscript III first strand synthesis system (Thermo Fisher). The cDNA encoding *Cst3* (accession NM_009976) was PCR amplified using the primers (restriction sites underlined) *Cst3*-BamF: GATGATGGATCCTTGTCCTAGCCAACCATGGCC and *Cst3*-XmaR: GATGATCCCGGGCCCTTAGGCATTTTTGCAGC and subcloned into pWPI (a gift from Didier Trono (Addgene plasmid number 12254)) that had been modified to contain specific BamHI and XmaI sites inserted at the PacI site on the original plasmid (pWPI-BSMX).

pWPI-*Cst3* or pWPI alone (empty vector) were packaged into lentiviral particles by co-transfecting HEK293FT cells (Thermo Fisher) with psPAX2 and pMD2.G (gifts from Didier Trono (Addgene plasmid numbers 12260 and 12259, respectively)). The viral particles were concentrated from the resulting cell culture supernatant in 25 × 89 mm ultracentrifuge tubes, underlayed with 2 mL 20% sucrose in PBS by ultracentrifugation at 50,000 × g for 2h using a SW28 rotor (Beckman Coulter, Indianapolis, IN). The viral pellet was resuspended in PBS and frozen in aliquots at −80°C. The titers were determined using the qPCR lentivirus titration kit and were generally ~10^8 IU/mL (Applied Biological Materials).

Primary female WT and *Cst3*$^{-/-}$ BMDMs were seeded into 24-well plates and transduced with 1 – 5 × 10^6 IU of either *Cst3* or empty vector lentivirus in the presence of 8μg/mL polybrene in fresh complete media for 16h. Following the incubation, the media was replaced with fresh complete media and the cells were incubated for an additional 3 to 5 days prior to 100ng/ml LPS stimulation for 24h.

QUANTIFICATION AND STATISTICAL ANALYSIS

Western blot densitometric quantification—Western blot bands were quantified using ImageJ 2.0.0 software. The optical density (OD) of an area around each band was obtained and a ratio of OD:area was calculated. The OD:area values for a protein of interest were then normalized to the corresponding actin OD:area ratio.

Immunohistochemical analysis—The entire area of the immunostained spinal cord was obtained at 20X magnification with an Olympus Slide Scanner microscope. The number of

$CD45^+$ profiles was obtained by selecting the entire area of tissue and highlighting positively labeled cells by using a fixed threshold of illumination for all samples. Four sections that were 50 μm apart from each other were quantified per mouse and three mice were counted per genotype. The cell infiltration counts were measured as cells counted per mouse/whole area per mouse.

Eriochrome cyanine analysis—Four sections that were 50 μm apart from each other were counted per mouse and three mice per genotype were quantified. The sections were imaged at 20X magnification with a slide scanner (Olympus). The entire euriochrome cyanine-stained area on every slide was outlined using cellSense 1.18 (Olympus). Demyelination was measured as demyelinated area per mouse/whole area per mouse.

Statistics—Statistical tests are indicated in the figure legends and were completed using GraphPad Prism 6 software (GraphPad, La Jolla, CA, USA) with $p < 0.05$ considered significant. All error bars represent SEM. EAE scoring was carried out by two investigators masked to the genotypes and treatments with all combined experiments shown. Cytokine results are displayed as single experiments or combined experiments where each dot represents each well normalized to its corresponding WT condition. All data points for the combined cytokine data are shown.

Supplementary Material

Refer to Web version on PubMed Central for supplementary material.

ACKNOWLEDGMENTS

This work was funded by operating grants to S.S.O. from the Canadian Institutes of Health Research (MOP-136890) and the Multiple Sclerosis Society of Canada (MSSOC) (EGID 1994). E.L. was funded by the National Institute on Aging (AG017617). V.H. was supported by a studentship from MSSOC. We thank Dr. Robin Yates for the 2D2 breeders and the L929 cell line and are grateful to the UK MS Tissue Bank for the human brain samples. We also thank Laurie Kennedy, Yiping Liu, and Lavinia Ionescu at the University of Calgary Flow Cytometry Facility and Amanda Scott from BD Life Sciences—Biosciences for guidance on the intracellular flow cytometry experiments.

REFERENCES

Aronica E, van Vliet EA, Hendriksen E, Troost D, Lopes da Silva FH, and Gorter JA (2001). Cystatin C, a cysteine protease inhibitor, is persistently upregulated in neurons and glia in a rat model for mesial temporal lobe epilepsy. Eur. J. Neurosci 14, 1485–1491. [PubMed: 11722610]

Bäcklund A, Holmdahl M, Mattsson R, Håkansson K, Lindström V, Nandakumar KS, Grubb A, and Holmdahl R (2011). Cystatin C influences the autoimmune but not inflammatory response to cartilage type II collagen leading to chronic arthritis development. Arthritis Res. Ther 13, R54. [PubMed: 21443774]

Bailey SL, Schreiner B, McMahon EJ, and Miller SD (2007). CNS myeloid DCs presenting endogenous myelin peptides 'preferentially' polarize CD4+ T(H)-17 cells in relapsing EAE. Nat. Immunol 8, 172–180. [PubMed: 17206145]

Beurel E, Harrington LE, Buchser W, Lemmon V, and Jope RS (2014). Astrocytes modulate the polarization of CD4+ T cells to Th1 cells. PLoS ONE 9, e86257. [PubMed: 24489707]

Chabas D, Baranzini SE, Mitchell D, Bernard CC, Rittling SR, Denhardt DT, Sobel RA, Lock C, Karpuj M, Pedotti R, et al. (2001). The influence of the proinflammatory cytokine, osteopontin, on autoimmune demyelinating disease. Science 294, 1731–1735. [PubMed: 11721059]

Chang TT, Jabs C, Sobel RA, Kuchroo VK, and Sharpe AH (1999). Studies in B7-deficient mice reveal a critical role for B7 costimulation in both induction and effector phases of experimental autoimmune encephalomyelitis. J. Exp. Med 190, 733–740. [PubMed: 10477557]

Cross AH, Girard TJ, Giacoletto KS, Evans RJ, Keeling RM, Lin RF, Trotter JL, and Karr RW (1995). Long-term inhibition of murine experimental autoimmune encephalomyelitis using CTLA-4-Fc supports a key role for CD28 costimulation. J. Clin. Invest 95, 2783–2789. [PubMed: 7539461]

Del Boccio P, Pieragostino D, Lugaresi A, Di Ioia M, Pavone B, Travaglini D, D'Aguanno S, Bernardini S, Sacchetta P, Federici G, et al. (2007). Cleavage of cystatin C is not associated with multiple sclerosis. Ann. Neurol 62, 201–204, discussion 205. [PubMed: 17006926]

Dudziak D, Kamphorst AO, Heidkamp GF, Buchholz VR, Trumpfheller C, Yamazaki S, Cheong C, Liu K, Lee H-W, Park CG, et al. (2007). Differential antigen processing by dendritic cell subsets in vivo. Science 315, 107–111. [PubMed: 17204652]

Dunn SE, Ousman SS, Sobel RA, Zuniga L, Baranzini SE, Youssef S, Crowell A, Loh J, Oksenberg J, and Steinman L (2007). Peroxisome proliferator-activated receptor (PPAR)alpha expression in T cells mediates gender differences in development of T cell-mediated autoimmunity. J Exp Med 204, 321–330. [PubMed: 17261635]

El-Sukkari D, Wilson NS, Hakansson K, Steptoe RJ, Grubb A, Shortman K, and Villadangos JA (2003). The protease inhibitor cystatin C is differentially expressed among dendritic cell populations, but does not control antigen presentation. J. Immunol 171, 5003–5011. [PubMed: 14607896]

Falsig J, Pörzgen P, Lund S, Schrattenholz A, and Leist M (2006). The inflammatory transcriptome of reactive murine astrocytes and implications for their innate immune function. J. Neurochem 96, 893–907. [PubMed: 16405499]

Fiorini M, Zanusso G, Benedetti MD, Righetti PG, and Monaco S (2007). Cerebrospinal fluid biomarkers in clinically isolated syndromes and multiple sclerosis. Proteomics Clin. Appl 1, 963–971. [PubMed: 21136750]

Frendéus KH, Wallin H, Janciauskiene S, and Abrahamson M (2009). Macrophage responses to interferon-gamma are dependent on cystatin C levels. Int. J. Biochem. Cell Biol 41, 2262–2269. [PubMed: 19446036]

Gauthier S, Kaur G, Mi W, Tizon B, and Levy E (2011). Protective mechanisms by cystatin C in neurodegenerative diseases. Front. Biosci. (Schol. Ed.) 3, 541–554. [PubMed: 21196395]

Gauthier SA, Tizon B, Sahoo S, and Levy E (2012). In vitro assays measuring protection by proteins such as cystatin C of primary cortical neuronal and smooth muscle cells. Methods Mol. Biol 849, 275–287. [PubMed: 22528097]

Giraud SN, Caron CM, Pham-Dinh D, Kitabgi P, and Nicot AB (2010). Estradiol inhibits ongoing autoimmune neuroinflammation and NFkappaB-dependent CCL2 expression in reactive astrocytes. Proc. Natl. Acad. Sci. USA 107, 8416–8421. [PubMed: 20404154]

Han MH, Hwang SI, Roy DB, Lundgren DH, Price JV, Ousman SS, Fernald GH, Gerlitz B, Robinson WH, Baranzini SE, et al. (2008). Proteomic analysis of active multiple sclerosis lesions reveals therapeutic targets. Nature 451, 1076–1081. [PubMed: 18278032]

Hansson SF, Simonsen AH, Zetterberg H, Andersen O, Haghighi S, Fagerberg I, Andréasson U, Westman-Brinkmalm A, Wallin A, Rüetschi U, and Blennow K (2007). Cystatin C in cerebrospinal fluid and multiple sclerosis. Ann. Neurol 62, 193–196, discussion 205. [PubMed: 16900522]

Haves-Zburof D, Paperna T, Gour-Lavie A, Mandel I, Glass-Marmor L, and Miller A (2011). Cathepsins and their endogenous inhibitors cystatins: expression and modulation in multiple sclerosis. J. Cell. Mol. Med 15, 2421–2429. [PubMed: 21143385]

Hayashi M, Luo Y, Laning J, Strieter RM, and Dorf ME (1995). Production and function of monocyte chemoattractant protein-1 and other beta-chemokines in murine glial cells. J. Neuroimmunol 60, 143–150. [PubMed: 7642742]

Huh CG, Hakansson K, Nathanson CM, Thorgeirsson UP, Jonsson N, Grubb A, Abrahamson M, and Karlsson S (1999). Decreased metastatic spread in mice homozygous for a null allele of the cystatin C protease inhibitor gene. Mol. Pathol 52, 332–340. [PubMed: 10748866]

Irani DN, Anderson C, Gundry R, Cotter R, Moore S, Kerr DA, McArthur JC, Sacktor N, Pardo CA, Jones M, et al. (2006). Cleavage of cystatin C in the cerebrospinal fluid of patients with multiple sclerosis. Ann. Neurol 59, 237–247. [PubMed: 16437581]

Itoh Y, Yamada M, Hayakawa M, Otomo E, and Miyatake T (1993). Cerebral amyloid angiopathy: a significant cause of cerebellar as well as lobar cerebral hemorrhage in the elderly. J. Neurol. Sci 116, 135–141. [PubMed: 8336159]

Kitamura H, Kamon H, Sawa S, Park SJ, Katunuma N, Ishihara K, Murakami M, and Hirano T (2005). IL-6-STAT3 controls intracellular MHC class II alphabeta dimer level through cathepsin S activity in dendritic cells. Immunity 23, 491–502. [PubMed: 16286017]

Lehmann CHK, Baranska A, Heidkamp GF, Heger L, Neubert K, Lühr JJ, Hoffmann A, Reimer KC, Brückner C, Beck S, et al. (2017). DC subset-specific induction of T cell responses upon antigen uptake via Fcγ receptors in vivo. J. Exp. Med 214, 1509–1528. [PubMed: 28389502]

Leung-Tack J, Tavera C, Martinez J, and Colle A (1990). Neutrophil chemotactic activity is modulated by human cystatin C, an inhibitor of cysteine proteases. Inflammation 14, 247–258. [PubMed: 2361732]

Levy E, Sastre M, Kumar A, Gallo G, Piccardo P, Ghetti B, and Tagliavini F (2001). Codeposition of cystatin C with amyloid-beta protein in the brain of Alzheimer disease patients. J. Neuropathol. Exp. Neurol 60, 94–104. [PubMed: 11202179]

Li W, Sultana N, Siraj N, Ward LJ, Pawlik M, Levy E, Jovinge S, Bengtsson E, and Yuan XM (2016). Autophagy dysfunction and regulatory cystatin C in macrophage death of atherosclerosis. J. Cell. Mol. Med 20, 1664–1672. [PubMed: 27079462]

Liva SM, and Voskuhl RR (2001). Testosterone acts directly on CD4+ T lymphocytes to increase IL-10 production. J. Immunol 167, 2060–2067. [PubMed: 11489988]

Lock C, Hermans G, Pedotti R, Brendolan A, Schadt E, Garren H, Langer-Gould A, Strober S, Cannella B, Allard J, et al. (2002). Gene-microarray analysis of multiple sclerosis lesions yields new targets validated in autoimmune encephalomyelitis. Nat. Med 8, 500–508. [PubMed: 11984595]

Maruyama K, Ikeda S, Ishihara T, Allsop D, and Yanagisawa N (1990). Immunohistochemical characterization of cerebrovascular amyloid in 46 autopsied cases using antibodies to beta protein and cystatin C. Stroke 21, 397–403. [PubMed: 2408196]

Matejuk A, Hopke C, Vandenbark AA, Hurn PD, and Offner H (2005). Middle-age male mice have increased severity of experimental autoimmune encephalomyelitis and are unresponsive to testosterone therapy. J. Immunol 174, 2387–2395. [PubMed: 15699175]

Mellman I, and Steinman RM (2001). Dendritic cells: specialized and regulated antigen processing machines. Cell 106, 255–258. [PubMed: 11509172]

Nagai A, Ryu JK, Terashima M, Tanigawa Y, Wakabayashi K, McLarnon JG, Kobayashi S, Masuda J, and Kim SU (2005). Neuronal cell death induced by cystatin C in vivo and in cultured human CNS neurons is inhibited with cathepsin B. Brain Res. 1066, 120–128. [PubMed: 16325785]

Nagai A, Terashima M, Sheikh AM, Notsu Y, Shimode K, Yamaguchi S, Kobayashi S, Kim SU, and Masuda J (2008). Involvement of cystatin C in pathophysiology of CNS diseases. Front. Biosci 13, 3470–3479. [PubMed: 18508448]

Nakashima I, Fujinoki M, Fujihara K, Kawamura T, Nishimura T, Nakamura M, and Itoyama Y (2007). Alteration of cystatin C in the cerebrospinal fluid of multiple sclerosis. Ann. Neurol 62, 197–200, discussion 205. [PubMed: 16958112]

Naves R, Singh SP, Cashman KS, Rowse AL, Axtell RC, Steinman L, Mountz JD, Steele C, De Sarno P, and Raman C (2013). The interdependent, overlapping, and differential roles of type I and II IFNs in the pathogenesis of experimental autoimmune encephalomyelitis. J. Immunol 191, 2967–2977. [PubMed: 23960239]

O'Connor RA, Prendergast CT, Sabatos CA, Lau CW, Leech MD, Wraith DC, and Anderton SM (2008). Cutting edge: Th1 cells facilitate the entry of Th17 cells to the central nervous system during experimental autoimmune encephalomyelitis. J. Immunol 181, 3750–3754. [PubMed: 18768826]

Olsson T, Nygren J, Håkansson K, Lundblad C, Grubb A, Smith ML, and Wieloch T (2004). Gene deletion of cystatin C aggravates brain damage following focal ischemia but mitigates the neuronal injury after global ischemia in the mouse. Neuroscience 128, 65–71. [PubMed: 15450354]

Orabona C, Grohmann U, Belladonna ML, Fallarino F, Vacca C, Bianchi R, Bozza S, Volpi C, Salomon BL, Fioretti MC, et al. (2004). CD28 induces immunostimulatory signals in dendritic cells via CD80 and CD86. Nat. Immunol 5, 1134–1142. [PubMed: 15467723]

Palaszynski KM, Smith DL, Kamrava S, Burgoyne PS, Arnold AP, and Voskuhl RR (2005). A yin-yang effect between sex chromosome complement and sex hormones on the immune response. Endocrinology 146, 3280–3285. [PubMed: 15905317]

Palm DE, Knuckey NW, Primiano MJ, Spangenberger AG, and Johanson CE (1995). Cystatin C, a protease inhibitor, in degenerating rat hippocampal neurons following transient forebrain ischemia. Brain Res. 691, 1–8. [PubMed: 8590041]

Papenfuss TL, Rogers CJ, Gienapp I, Yurrita M, McClain M, Damico N, Valo J, Song F, and Whitacre CC (2004). Sex differences in experimental autoimmune encephalomyelitis in multiple murine strains. J. Neuroimmunol 150, 59–69. [PubMed: 15081249]

Patterson NL, and Mintern JD (2012). Intersection of autophagy with pathways of antigen presentation. Protein Cell 3, 911–920. [PubMed: 23136066]

Pawlik M, Sastre M, Calero M, Mathews PM, Schmidt SD, Nixon RA, and Levy E (2004). Overexpression of human cystatin C in transgenic mice does not affect levels of endogenous brain amyloid Beta Peptide. J. Mol. Neurosci 22, 13–18. [PubMed: 14742906]

Petković F, and Castellano B (2016). The role of interleukin-6 in central nervous system demyelination. Neural Regen. Res 11, 1922–1923. [PubMed: 28197184]

Pierre P, and Mellman I (1998). Developmental regulation of invariant chain proteolysis controls MHC class II trafficking in mouse dendritic cells. Cell 93, 1135–1145. [PubMed: 9657147]

Ramien C, Taenzer A, Lupu A, Heckmann N, Engler JB, Patas K, Friese MA, and Gold SM (2016). Sex effects on inflammatory and neurodegenerative processes in multiple sclerosis. Neurosci. Biobehav. Rev 67, 137–146. [PubMed: 26773723]

Rodriguez-Franco EJ, Cantres-Rosario YM, Plaud-Valentin M, Romeu R, Rodríguez Y, Skolasky R, Meléndez V, Cadilla CL, and Melendez LM (2012). Dysregulation of macrophage-secreted cathepsin B contributes to HIV-1-linked neuronal apoptosis. PLoS ONE 7, e36571. [PubMed: 22693552]

Solem M, Rawson C, Lindburg K, and Barnes D (1990). Transforming growth factor beta regulates cystatin C in serum-free mouse embryo (SFME) cells. Biochem. Biophys. Res. Commun 172, 945–951. [PubMed: 2241983]

Tizon B, Ribe EM, Mi W, Troy CM, and Levy E (2010a). Cystatin C protects neuronal cells from amyloid-beta-induced toxicity. J. Alzheimers Dis 19, 885–894. [PubMed: 20157244]

Tizon B, Sahoo S, Yu H, Gauthier S, Kumar AR, Mohan P, Figliola M, Pawlik M, Grubb A, Uchiyama Y, et al. (2010b). Induction of autophagy by cystatin C: a mechanism that protects murine primary cortical neurons and neuronal cell lines. PLoS ONE 5, e9819. [PubMed: 20352108]

Touahri Y, Adnani L, Mattar P, Markham K, Klenin N, and Schuurmans C (2015). Non-isotopic RNA In Situ Hybridization on Embryonic Sections. Curr. Protoc. Neurosci 70, 1.22.21–1.22.25. [PubMed: 25559002]

Verdot L, Lalmanach G, Vercruysse V, Hartmann S, Lucius R, Hoebeke J, Gauthier F, and Vray B (1996). Cystatins up-regulate nitric oxide release from interferon-gamma-activated mouse peritoneal macrophages. J. Biol. Chem 271, 28077–28081. [PubMed: 8910420]

Vinters HV, Nishimura GS, Secor DL, and Pardridge WM (1990). Immunoreactive A4 and gamma-trace peptide colocalization in amyloidotic arteriolar lesions in brains of patients with Alzheimer's disease. Am. J. Pathol 137, 233–240. [PubMed: 2201197]

Voskuhl RR, and Palaszynski K (2001). Sex hormones in experimental autoimmune encephalomyelitis: implications for multiple sclerosis. Neuroscientist 7, 258–270. [PubMed: 11499404]

Wang F, and Muller S (2015). Manipulating autophagic processes in autoimmune diseases: a special focus on modulating chaperone-mediated autophagy, an emerging therapeutic target. Front. Immunol 6, 252. [PubMed: 26042127]

Wang X, Deckert M, Xuan NT, Nishanth G, Just S, Waisman A, Naumann M, and Schlüter D (2013). Astrocytic A20 ameliorates experimental autoimmune encephalomyelitis by inhibiting NF-kappaB- and STAT1-dependent chemokine production in astrocytes. Acta Neuropathol. 126, 711–724. [PubMed: 24077734]

Warfel AH, Zucker-Franklin D, Frangione B, and Ghiso J (1987). Constitutive secretion of cystatin C (gamma-trace) by monocytes and macrophages and its downregulation after stimulation. J. Exp. Med 166, 1912–1917. [PubMed: 3119764]

Xie L, Choudhury GR, Winters A, Yang SH, and Jin K (2015). Cerebral regulatory T cells restrain microglia/macrophage-mediated inflammatory responses via IL-10. Eur. J. Immunol 45, 180–191. [PubMed: 25329858]

Xu L, Sheng J, Tang Z, Wu X, Yu Y, Guo H, Shen Y, Zhou C, Paraoan L, and Zhou J (2005). Cystatin C prevents degeneration of rat nigral dopaminergic neurons: in vitro and in vivo studies. Neurobiol. Dis 18, 152–165. [PubMed: 15649706]

Ziehn MO, Avedisian AA, Dervin SM, Umeda EA, O'Dell TJ, and Voskuhl RR (2012). Therapeutic testosterone administration preserves excitatory synaptic transmission in the hippocampus during autoimmune demyelinating disease. J. Neurosci 32, 12312–12324. [PubMed: 22956822]

Zucker-Franklin D, Warfel A, Grusky G, Frangione B, and Teitel D (1987). Novel monocyte-like properties of microglial/astroglial cells. Constitutive secretion of lysozyme and cystatin-C. Lab. Invest 57, 176–185. [PubMed: 3302535]

Highlights

- Cystatin C (CST3) has a detrimental role in $MOG_{35–55}$-induced EAE but only in female mice
- Activation of female but not male antigen-presenting cells is promoted by CST3
- CST3 in antigen-presenting cells is associated with activation of female CD4 T cells
- The sex-dependent effect of CST3 in EAE is sensitive to gonadal hormones

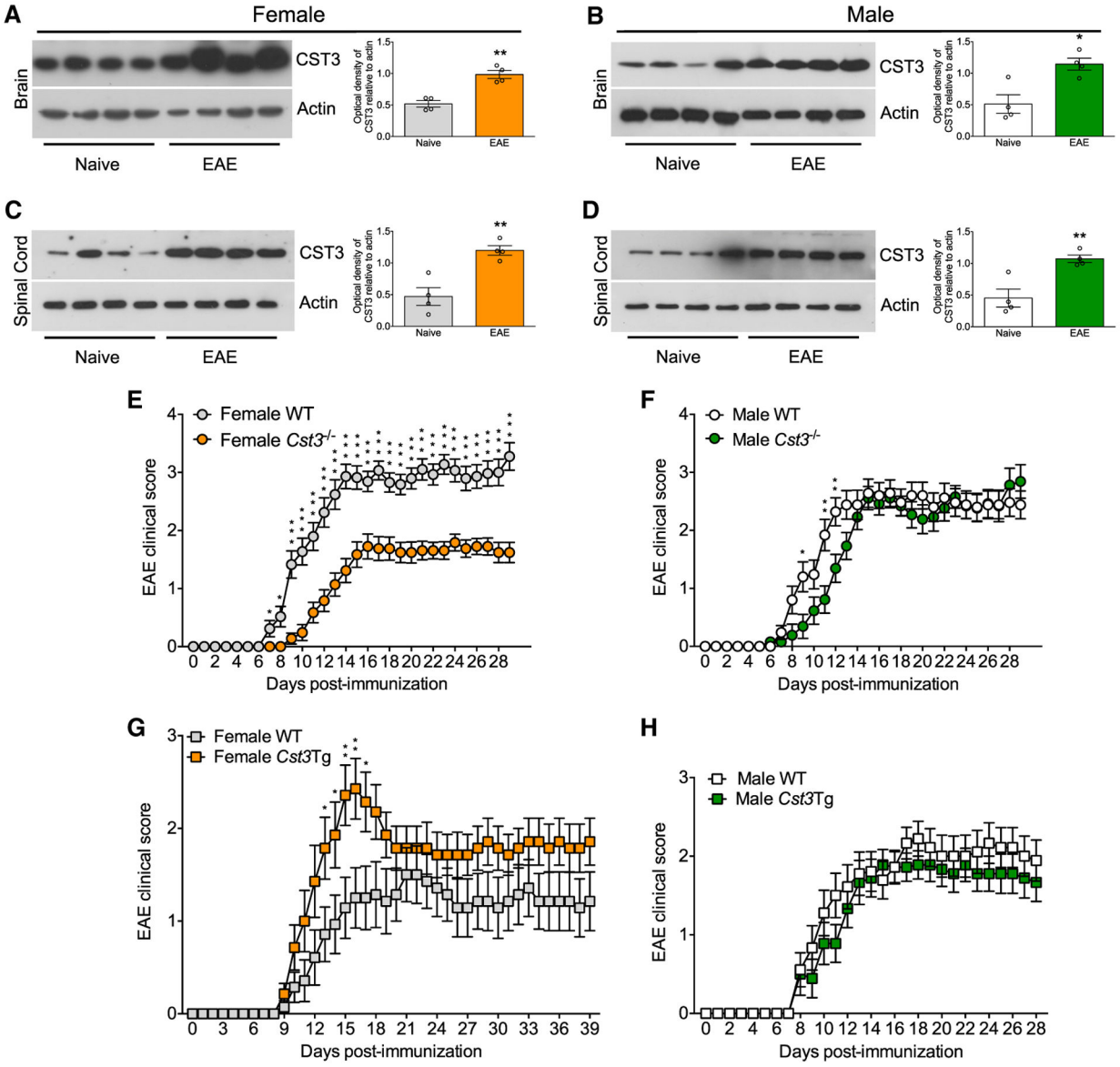

Figure 1. CST3 Is Detrimental in Female EAE Mice

(A–D) Western blots and semi-quantification of CST3 (~13 kDa) and actin (~42 kDa) levels in brains (A and B) and spinal cords (C and D) from naive and d14 EAE female (A and C) and male (B and D) C57BL/6J mice. Each lane represents an individual mouse. Bar graphs represent mean ± SEM. Two-tailed unpaired Student's t test: *p < 0.05; **p < 0.01.

(E–H) EAE clinical signs in female (E and G) and male (F and H) *Cst3*$^{-/-}$ (orange/green circles) versus WT (gray/white circles) mice (E and F) and *Cst3*Tg (orange/green squares) versus WT (gray/white squares) littermates (G and H). Results expressed as mean EAE score ± SEM and represent three combined WT versus *Cst3*$^{-/-}$ and two combined WT versus *Cst3*Tg experiments. *p < 0.05; **p < 0.01; ***p < 0.001, repeated-measures two-way ANOVA with Šídák post hoc test; n = 29 (WT versus *Cst3*$^{-/-}$) and 25 (WT versus *Cst3*Tg) mice per group.

See also Figure S1 and Tables S1–S3.

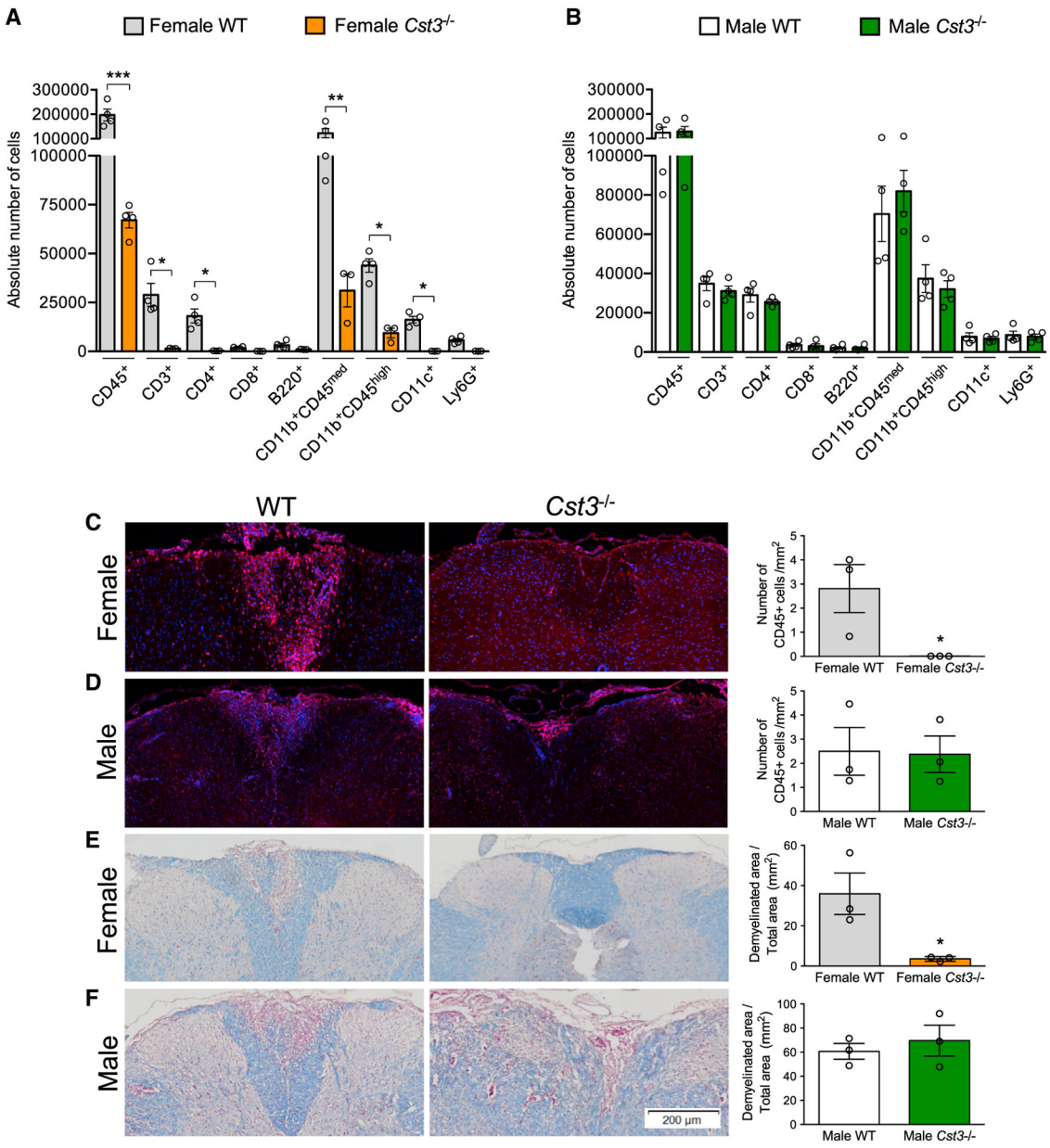

Figure 2. CST3 Promotes Inflammation in Female EAE Mice

(A and B) Flow-cytometric analysis of the absolute number of $CD45^+$ immune cells; $CD3^+$, $CD4^+$, and $CD8^+$ T cells; $B220^+$ B cells; $CD11b^+CD45^{med}$ microglia; $CD11b^+$ $CD45^{high}$ macrophages; $CD11c^+$ dendritic cells; and $Ly6G^+$ neutrophils present in the spinal cords of female (A) and male (B) WT (gray/white bars) and *Cst3*$^{-/-}$ (orange/green bars) EAE mice. Results are expressed as mean ± SEM; n = 4 individual mice/group. One-way ANOVA: *p < 0.05; **p < 0.01; ***p < 0.001.

(C–F) Micrographs (scale bar, 200 µm) and quantifications of the number of $CD45^+$ cells (C and D) and amount of demyelination (E and F) in female (C and E) and male (D and F) WT and *Cst3*$^{-/-}$ EAE mice. n = 3 mice per group. Two-tailed unpaired Student's t test: *p < 0.05.

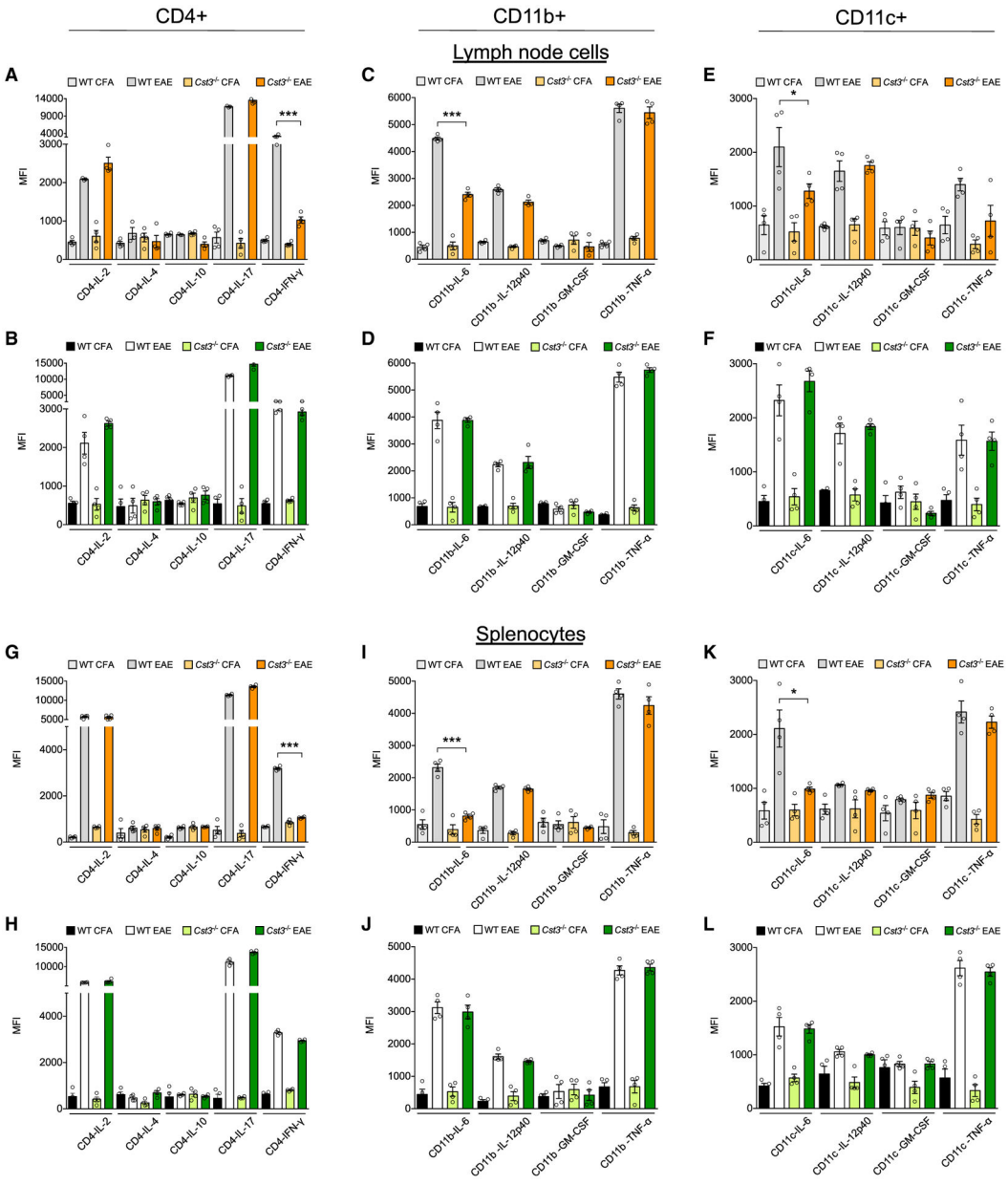

Figure 3. CST3 Promotes IL-6 and IFN-γ Cytokine Expression in Lymph Node and Spleen Immune Cells from Female EAE Mice

(A–L) Mean fluorescence intensity (MFI) of various cytokines present within $CD4^+$ (A, B, G, and H), $CD11b^+$ (C, D, I, and J) and $CD11c^+$ (E, F, K, and L) lymph-node-derived (A–F) and spleen-derived (G–L) immune cells from female (A, C, E, G, I, and K) and male (B, D, F, H, J, and L) WT (gray/white/black bars) and *Cst3*$^{-/-}$ (orange/green bars) CFA and EAE mice. Data are represented as mean ± SEM with 4 individual animals per group. One-way ANOVA with Šídák post hoc test: *$p < 0.05$; ***$p < 0.001$.

See also Figure S2.

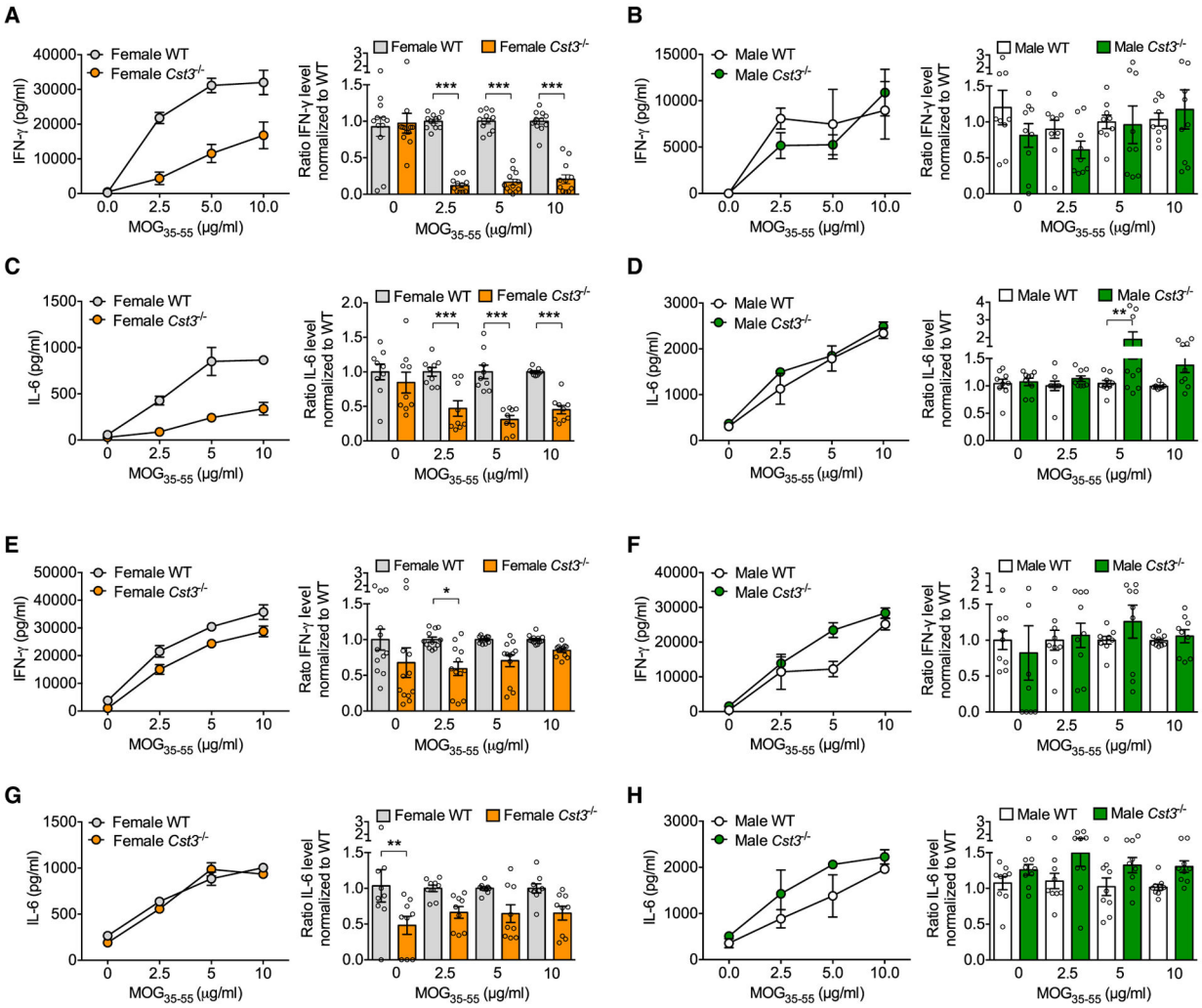

Figure 4. CST3 Promotes IL-6 and IFN-γ Cytokine Secretion by Female EAE Splenocytes

(A–H) IFN-γ (A, B, E, and F) and IL-6 (C, D, G, and H) production by female (A, C, E, and G) and male (B, D, F, and H) $MOG_{35–55}$-stimulated WT (gray/white bars) and *Cst3*$^{-/-}$ (orange/green bars) EAE splenocytes (A–D) and lymph node cells (E–H). Line graphs represent one experiment consisting of cells pooled from 3 or 5 mice for each group and triplicate wells plated for each condition. Bar graph data represent mean ± SEM and are a combination of 4 separate experiments. Each dot represents each well and indicates the ratio of that well normalized to its corresponding WT condition. One-way ANOVA with Šídák post hoc test: *$p < 0.05$; **$p < 0.01$; ***$p < 0.001$.

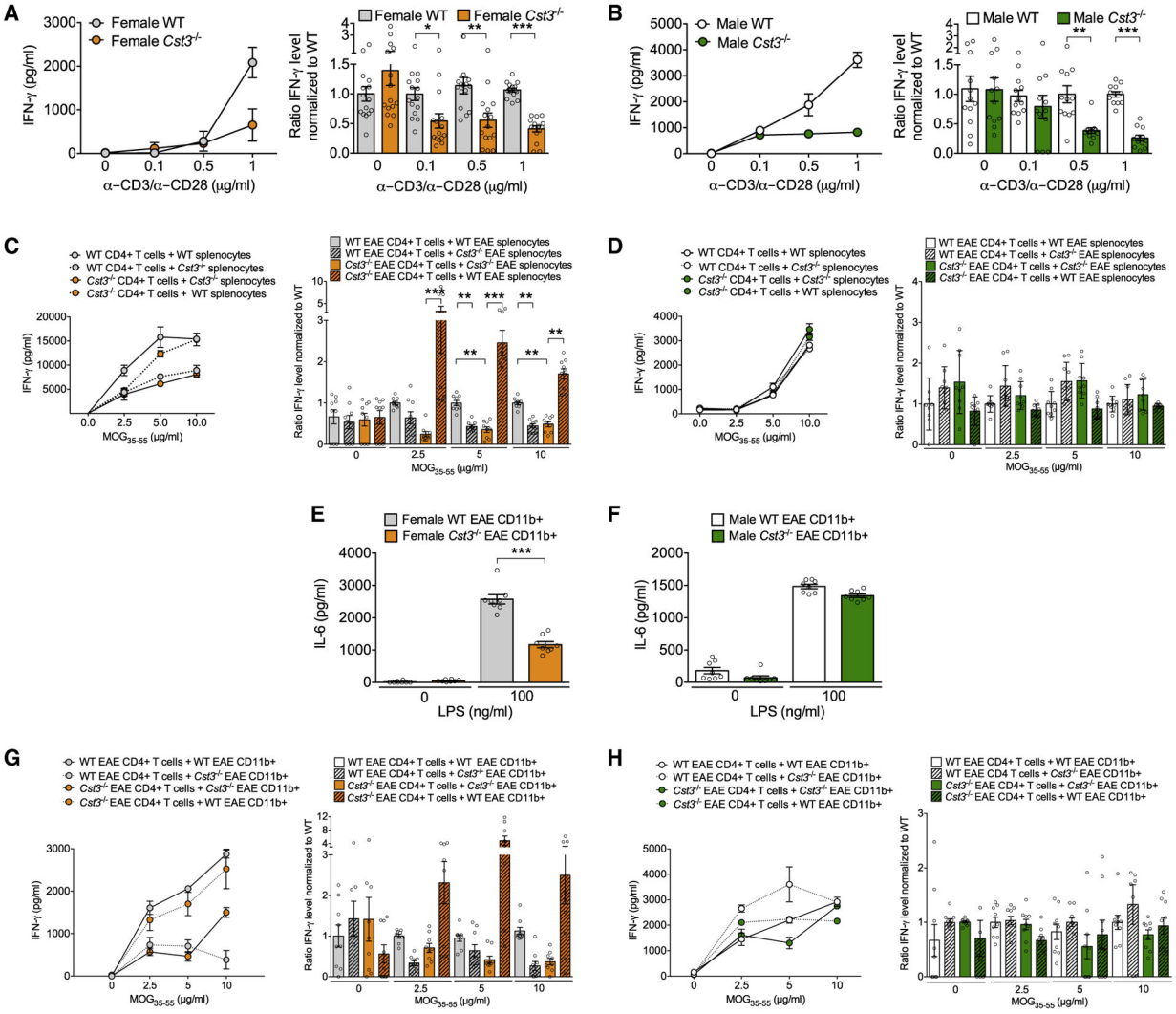

Figure 5. CST3 Promotes Activation of APCs in Female EAE Mice

(A and B) IFN-γ profile in female (A) and male (B) WT (gray/white bars) and *Cst3*$^{-/-}$ (orange/green bars) CD4^{+} T cells activated with anti-CD3/anti-CD28.

(C and D) EAE splenic CD4^{+} T cells co-cultured with syngeneic (solid bars) or alternate-genotype (patterned bars) EAE splenocytes from female (C) and male (D) WT (gray/white) and *Cst3*$^{-/-}$ (orange/green) mice.

(E and F) IL-6 production by female (E) and male (F) WT (gray/white) and *Cst3*$^{-/-}$ (orange/green) spleen-derived EAE CD11b^{+} cells stimulated with LPS.

(G and H) IFN-γ secretion by female (G) and male (H) WT (gray/white) and *Cst3*$^{-/-}$ (orange/green) spleen-derived EAE CD4^{+} T cells co-cultured with syngeneic (solid bars) or alternate-genotype (patterned bars) EAE CD11b^{+} cells.

In (A–D), (G), and (H) line graphs represent one experiment consisting of cells pooled from 3 or 5 mice for each group and triplicate wells plated for each condition. Bar graphs are presented as mean ± SEM and display the combination of 3 separate experiments. Each dot represents each well and indicates the ratio of that well normalized to its corresponding WT condition. One-way ANOVA with Šídák post hoc test. In (E) and (F), data are presented

as mean ± SEM and represent 4 individual mice with duplicate wells plated. Two-tailed unpaired Student's t test: *$p < 0.05$; **$p < 0.01$; ***$p < 0.001$.
See also Figures S3 and S4.

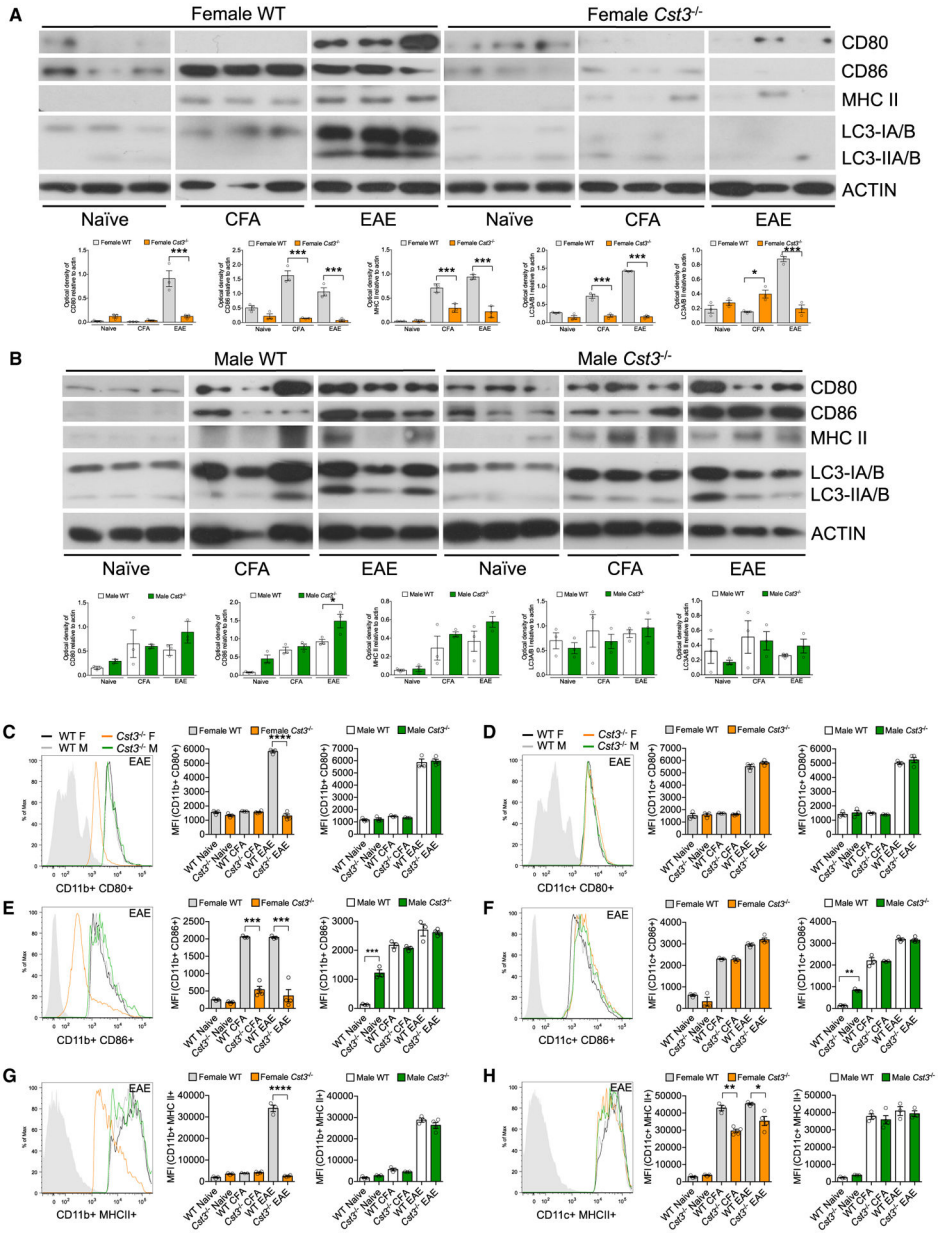

Figure 6. CST3 Promotes the Expression of Antigen-Processing and Antigen Presentation Molecular Markers in female CD11b$^+$ Cells

(A and B) Western blots and semi-quantification of CD80, CD86, MHC II, and LC3A/BI/II levels in female (A) and male (B) naive, CFA, and d6 EAE-derived WT (gray/white) and *Cst3*$^{-/-}$ (orange/green) splenic CD11b$^+$ cells. Data represent one of three experiments with graphs displaying the mean ± SEM of 3 individual mice. Repeated-measures two-way ANOVA with Šídák post hoc test: *$p < 0.05$; **$p < 0.01$; ***$p < 0.001$.

(C–H) MFI of CD80 (C and D), CD86 (E and F), and MHC II (G and H) expression in female (gray/orange) and male (white/green) WT (gray/white bars) and *Cst3*$^{-/-}$ (orange/green bars) spleen-derived CD11b$^+$ (C, E, and G) and CD11c$^+$ (D, F, and H) cells from naive, CFA and EAE mice. Data are displayed as mean ± SEM and represent 3–4 individual

animals per group. One-way ANOVA with Šídák post hoc test: *p < 0.05, **p < 0.01, ***p < 0.001; ****p < 0.0001.

See also Figures S5–S7.

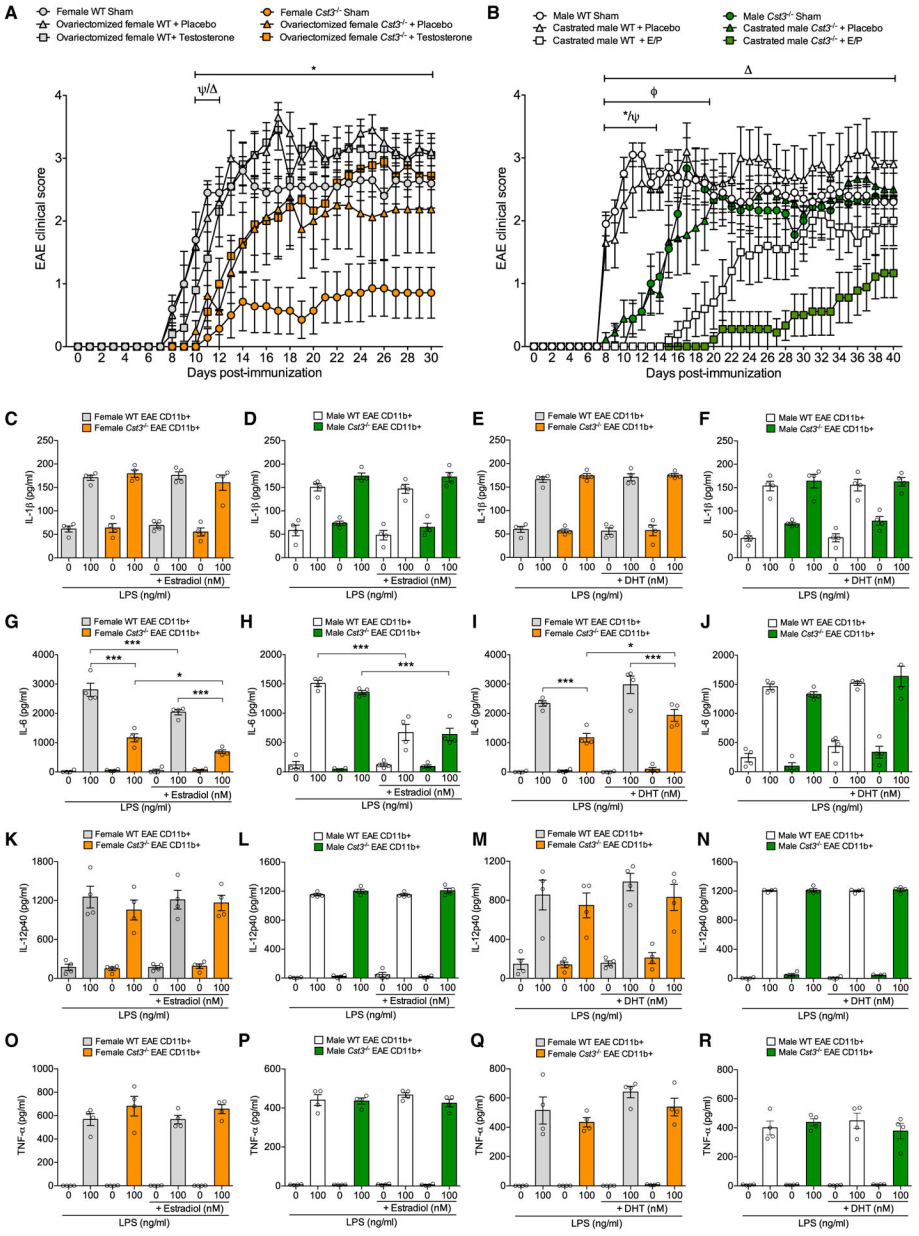

Figure 7. Estrogen/Progesterone (E/P) Is Involved in CST3's Sex-Dependent Effect in CD11b$^+$ Cell Activation and EAE Disability

(A and B) EAE disability in ovariectomized female WT (gray) and *Cst3*$^{-/-}$ (orange) mice treated with testosterone (A), and castrated male WT (white) and *Cst3*$^{-/-}$ (green) mice administered E/P (B). Results are expressed as mean EAE score ± SEM; n = 8–10 mice per group; two-way ANOVA with Šídák post hoc test, p range < 0.05–0.001; Comparisons made: *,WT sham versus *Cst3*$^{-/-}$ sham; Ω, WT sham versus WT castrated/ovariectomized + placebo; ψ, WT sham versus *Cst3*$^{-/-}$ castrated/ovariectomized + placebo; ϕ, WT sham versus WT castrated/ovariectomized + E/P or testosterone; Δ,WT sham versus *Cst3*$^{-/-}$ castrated/ovariectomized + E/P or testosterone.

(C–R) IL-1β (C–F), IL-6 (G–J), IL-12p40 (K–N), and TNF-α (O–R) production by splenic CD11b$^+$ cells from EAE female (C, E, G, I, K, M, O, and Q) and male (D, F, H, J, L, N,

P, and R) WT (gray/white) and *Cst3*$^{-/-}$ (orange/green) mice cultured with 17-β estradiol or DHT ± LPS. Data are presented as mean ± SEM and represent four individual mice per condition. Two-way ANOVA with Šídák post hoc test: *$p < 0.05$; ***$p < 0.001$.
See also Figure S8 and Tables S5 and S6.

KEY RESOURCES TABLE

REAGENT or RESOURCE	SOURCE	IDENTIFIER
Antibodies		
Hamster anti-mouse CD3e (Clone 145–2C11)	BD	Cat # 553058
NA/LE hamster anti-mouse CD28 (Clone 37.51)	BD	Cat # 553294
Mouse anti-Cystatin C	R&D Systems	Cat # MAB1238
Rabbit anit-actin	Millipore Sigma	Cat # A2066
Rabbit anti-mouse CD86	abcam	Cat # ab112490
Rabbit anti-mouse LC3A (D50G8) XP	Cell Signaling	Cat # 4599
Rabbit anti-mouse MHC Class II	abcam	Cat # ab180779
Anti-mouse B7–1/CD80 (Clone 111114)	R&D Systems	Cat # MAB740
Rat anti-mouse CD45 (Clone 30-F11)	BD	Cat # 550539
Rat anti-mouse CD45, APC-Cy7 (Clone 30-F11)	BD	Cat # 557659
Rat anti-mouse CD45, APC (Clone 30-F11)	BD	Cat # 559864
Rat anti-mouse CD45, PerCP (Clone 30-F11)	BD	Cat # 557235
Hamster anti-mouse CD3e, BV711 (Clone 145–2C11)	BD	Cat # 563123
Hamster anti-mouse CD3e, FITC (Clone 145–2C11)	BD	Cat # 553062
Hamster anti-mouse CD3e, APC (Clone 145–2C11)	BD	Cat # 553066
Rat anti-mouse CD4, BV786 (Clone RM4–5)	BD	Cat # 563234
Rat anti-mouse CD4, FITC (Clone RM4–5)	BD	Cat # 553047
Rat anti-mouse CD4, PerCP (Clone RM4–5)	BD	Cat # 553052
Rat anti-mouse CD8α, BV650 (Clone 53–6.7)	BD	Cat # 563234
Rat anti-mouse CD8α, PE (Clone 53–6.7)	BD	Cat # 553032
Rat anti-CD11b, FITC	BD	Cat # 553310
Rat anti-CD11b, BV650	BD	Cat # 563402
Rat anti-CD11b, BV421	BD	Cat # 562605
Rat anti-CD11b, APC	BD	Cat # 553312
Hamster anti-mouse CD11c, APC (Clone HL3)	BD	Cat # 550261
Hamster anti-mouse CD11c, BV510 (Clone HL3)	BD	Cat # 562949
Hamster anti-mouse CD11c, AlexaFluor700 (Clone HL3)	BD	Cat # 560583
Rat anti-mouse CD45R/B220, BV786 (Clone RA3–6B2)	BD	Cat # 563894
Rat anti-mouse CD45R/B220, FITC (Clone RA3–6B2)	BD	Cat # 553087
Rat anti-mouse CD45R/B220, BV421 (Clone RA3–6B2)	BD	Cat # 562922
Rat anti-mouse Ly-6G, PerCP-Cy5.5 (Clone 1A8)	BD	Cat # 560602
Rat anti-mouse Ly-6G, FITC (Clone 1A8)	BD	Cat # 551460
Hamster anti-mouse CD80, PE (Clone 16–10A1)	BD	Cat # 553769
Rat anti-mouse CD86, PE-Cy7 (Clone GL1)	BD	Cat # 560582
Rat anti-mouse I-A/I-E, PerCP-Cy5.5 (Clone M5/114.15.2)	BD	Cat # 562363
Rat anti-mouse IL-2, AlexaFluor488 (Clone JES6–5H4)	BD	Cat # 557725
Rat anti-mouse IFN-γ, PE (Clone XMG1.2)	BD	Cat # 554412
Rat anti-mouse IL-4, AlexaFluor647 (Clone 11B11)	BD	Cat # 557739

REAGENT or RESOURCE	SOURCE	IDENTIFIER
Rat anti-mouse IL-17A, BV786 (Clone TC11–18H10)	BD	Cat # 564171
Rat anti-mouse IL-10, BV421 (Clone JES5–16E3)	BD	Cat # 563276
Rat anti-mouse GM-CSF, BV421 (Clone MP1–22E9)	BD	Cat # 564747
Rat anti-mouse TNF, BV711 (Clone MP6-XT22)	BD	Cat # 563944
Rat anti-mouse IL-12 (p40/p70), FITC (Clone C15.6)	BD	Cat # 560564
Rat anti-mouse IL-6, APC (Clone MP5–20F3)	BD	Cat # 561367
Bacterial and Virus Strains		
Human MS brain samples	United Kingdom Multiple Sclerosis Society Tissue Bank	https://www.mssociety.org.uk/research/explore-our-research/research-we-fund/search-our-research-projects/ms-society-tissue-bank
Chemicals, Peptides, and Recombinant Proteins		
Myelin oligodendrocyte glycoprotein 35–55 peptide	Stanford University Pan Facility	http://pan.stanford.edu/index.html
Mycobacterium Tuberculosis H37Ra (BD Difco Adjuvants)	Fisher Scientific	Cat # DF3114-33-8
Incomplete Freund's adjuvant (BD Difco Adjuvants)	Fisher Scientific	Cat # DF0639-60-6
Bordetella pertussis toxin (salt-free)	List Biological Laboratories, Inc.	Cat # 181
Thioglycollate prepared media	Fisher Scientific	Cat # BB21195
Fetal bovine serum, charcoal stripped	Thermo Fisher Scientific	Cat # 12676029
Recombinant mouse IFN-γ protein	Thermo Fisher Scientific	Cat # PMC4031
4-androsten-17β-OL-3-one (Testosterone)	Steraloids	Cat # A6950–000
17β-estradiol + progesterone pellets	Innovative Research of America	Cat # NHH-112
Estradiol/progesterone placebo pellets	Innovative Research of America	Cat # C-111
β-Estradiol	Millipore Sigma	Cat # E2758
5α-Dihydroxytestosterone	Millipore Sigma	Cat # D-073
Critical Commercial Assays		
Mouse CD4 microbeads (L3T4)	Miltenyi Biotec	Cat # 130-117-043
Human and mouse CD11b microbeads	Miltenyi Biotec	Cat # 130-049-601
Mouse IL-1β ELISA set	BD	Cat # 559603
Mouse IL-2 ELISA set	BD	Cat # 555148
Mouse IL-4 ELISA set	BD	Cat # 555232
Mouse IL-6 ELISA set	BD	Cat # 555240
Mouse IL-10 ELISA set	BD	Cat # 555252
Mouse IL-12p40 ELISA set	BD	Cat # 555165
Mouse IL-17 DuoSet ELISA	R&D Systems	Cat # DY421
Mouse IFN-γ ELISA set	BD	Cat # 555138
Mouse TNF DuoSet ELISA	R&D Systems	Cat # DY410
REPLI-g single cell RNA library kit	QIAGEN	Cat # 150073
GeneRead adaptor I set 12-plex	QIAGEN	Cat # 180985
NextSeq 500 High Output v2 Kit (75 cycles)	Illumina	Cat # FC-404–2005

REAGENT or RESOURCE	SOURCE	IDENTIFIER
Cytofix/Cytoperm plus fixation/permeabilization kit (GolgiStop)	BD	Cat # 554715
Cytofix/Cytoperm plus fixation/permeabilization kit (GolgiPlug)	BD	Cat # 555028
Deposited Data		
Raw and analyzed data	This paper; NCBI GEO database repository	GEO Database: GSE157624; https://www.ncbi.nlm.nih.gov/geo/query/acc.cgi?acc=GSE157624
Experimental Models: Cell Lines		
HEK293FT	Thermo Fisher Scientific	Cat # R70007
Experimental Models: Organisms/Strains		
Cystatin C knockout mice	Dr. Anders Grubb	Lund University
Cystatin C overexpressing mice	Dr. Efrat Levy	New York University
2D2 mice (C57BL/6-Tg(Tcra2D2,Tcrb2D2) 1Kuch/J)	Jackson Laboratories	Cat # 006912
Software and Algorithms		
Prism 6	GraphPad	https://www.graphpad.com/scientific-software/prism/
cellSens 1.18	Olympus Life Science	https://www.olympus-lifescience.com/en/software/cellsens/
NIH ImageJ 2.0.0	NIH	https://imagej.nih.gov/ij/download.html
FlowJo 9.9.4	BD	https://www.flowjo.com/
Ingenuity pathway analysis	QIAGEN	https://www.qiagen.com/us/products/discovery-and-translational-research/next-generation-sequencing/informatics-and-data/interpretation-content-databases/ingenuity-pathway-analysis/?clear=true#orderinginformation